Smart electrode surfaces by electrolyte immobilization for electrocatalytic CO 2 conversion

Elli Vichou, Yanis Adjez, Yun Li, Maria Gómez-Mingot, Marc Fontecave, Carlos M Sánchez-Sánchez

Smart electrode surfaces by electrolyte immobilization for electrocatalytic CO_2 conversion

Elli Vichou[†,‡], Yanis Adjez[‡], Yun Li[†], Maria Gomez-Mingot[†,], Marc Fontecave[†,*] and Carlos M. Sánchez-Sánchez[‡,*]*

[†]Laboratoire de Chimie des Processus Biologiques, Collège de France, UMR 8229 CNRS, Sorbonne Université, PSL Research University, 11 Place Marcelin Berthelot, 75005 Paris, France

[‡]Sorbonne Université, CNRS, Laboratoire Interfaces et Systèmes Electrochimiques, LISE, 4 Place Jussieu, 75005 Paris, France

KEYWORDS: CO_2 Electroreduction; Imidazolium cation; Modified Electrodes; Molecular Catalyst; Local Electric Field

TOC

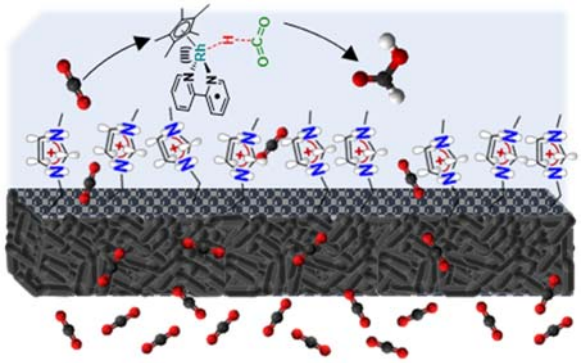

A surface-modified gas diffusion electrode combined with a molecular catalyst converts CO_2 into formate at high rate in water.

ABSTRACT

The activity and selectivity of molecular catalysts for the electrochemical CO_2 reduction reaction (CO_2RR) are influenced by the induced electric field at the electrode/electrolyte interface. We present here a novel electrolyte immobilization method to control the electric field at this interface by positively charging the electrode surface with an imidazolium cation organic layer, which significantly favors CO_2 conversion to formate, suppresses hydrogen evolution reaction (HER) and diminishes the operating cell voltage. Those results are well supported by our previous DFT calculations studying the mechanistic role of imidazolium cations in solution for CO_2 reduction to formate catalyzed by a model molecular catalyst. This smart electrode surface concept based on covalent grafting of imidazolium on a carbon electrode is successfully scaled up for operating at industrially relevant conditions (100 mA cm^{-2}) on an imidazolium-modified carbon-based gas diffusion electrode using a flow cell configuration, where the CO_2 conversion to formate process takes place in acidic aqueous solution to avoid carbonate formation and is catalyzed by a model molecular Rh complex in solution. The formate production rate reaches a maximum of 4.6 g_{HCOO^-} m^{-2} min^{-1} after accumulating a total of 9000 C of charge circulated on the same electrode. Constant formate production and no significant microscopic changes on the imidazolium-modified cathode in consecutives long-term CO_2 electrolysis confirmed the high stability of the imidazolium organic layer under operating conditions for CO_2RR.

INTRODUCTION

Controlling activity and selectivity in catalytic reactions by applying local electric fields (LEFs) as "reagents" has been already achieved in some reactions such as Diels-Alder cycloadditions[1]. LEFs can be designed by embedding charges into the reacting molecules for driving a million-fold catalytic enhancement such as in the case of organometallic complexes[2]. Furthermore, LEFs can be generated by controlling the type and the concentration of ions present in solution, a concept especially relevant in electrochemical reactions[3], since the electron transfer occurs at the polarizable electrode-electrolyte interface[4]. The key role of anions in solution enhancing the performance of palladium catalysts for oxidative cross-coupling reactions is one of the first reported examples of LEF effect in electrochemistry[5]. Furthermore, the impact of alkali metal cations in the electrolyte on the activity and selectivity of electrochemical carbon dioxide reduction reaction (CO_2RR) has been well documented in the literature[6–11]. This represents another relevant application of LEF for tuning an electrochemical reaction, since a higher concentration of cations likely accumulate at the interface with increasing cation size leading to a more powerful LEF[12]. Accordingly, total absence of CO_2RR activity on Cu, Ag and Au electrodes was reported when electrolysis was carried out in the absence of alkali metal cations in acidic solution[13,14]. The role of those cations is likely associated with the stabilization of negatively charged CO_2RR intermediates by favorable electrostatic interactions at the electrode-electrolyte interface, as well as the inhibition of proton adsorption and reduction[13]. Based on those findings, a cation-augmenting layer of K^+ on Cu electrode surface was recently proposed to overcome the limitation imposed by the solubility of alkali metal salts in aqueous solution, reaching an enhanced CO_2RR performance[14].

Nowadays, formate production by electrochemical means from CO_2, water and renewable energy represents one of the most developed and sustainable approaches for recycling CO_2[15]. Moreover, formate might work as hydrogen gas carrier, syngas storage medium and carbon source for bioprocesses, as well as an additive in the food industry, leather tanning, rubber production and as an intermediate in the chemical and pharmaceutical industry[16]. Recently we engaged a program aiming at optimizing molecular catalysts for CO_2 electroreduction to formate, via electrolyte and carbon electrode engineering. For that purpose, we got inspired by research efforts on heterogeneous CO_2RR focused on identifying new stabilizing cationic species, different from alkali metal cations[17], which would generate more powerful LEFs at the electrode-electrolyte interface and present larger stabilizing effect on reaction intermediates. In line with this view, we have recently reported the favorable electrostatic effect of imidazolium

cations from ionic liquids (ILs) in solution in order to enhance the activity of molecular catalysts for CO_2RR, resulting in diminished required overpotentials and enhancing selectivity in formate production *vs.* hydrogen evolution reaction (HER) in aqueous solution[18]. In particular, 1-ethyl-3-methylimidazolium cation ($[EMIM]^+$, **Figure 1a**) was demonstrated to tune the activity and selectivity of CO_2RR to formate catalyzed by a homogenous Rh complex ([Rh(bpy)(Cp*)Cl]Cl, complex **1**, with bpy = bipyridine and Cp* = pentamethylcyclopentadienyl, **Figure 1b**) in acidic aqueous solution[18] (**Figure 1c**). However, using ILs in solution presents some drawbacks for scaling up the process successfully due to their limited solubility in aqueous media, moderate ecotoxicity, high viscosity and cost. We propose here a new strategy, by which we shifted from electrolyte to electrode engineering, wherein small amounts of IL are immobilized on a carbon electrode surface by different methods, and the impact of these new modified carbon electrodes on the electrocatalytic properties of a homogenous molecular catalyst for CO_2RR, namely complex **1**, are evaluated. This electrode engineering alternative not only allows nicely overcoming the above-mentioned limitations, but also provides insights into novel modified carbon-based electrodes for CO_2RR catalyzed by molecular complexes. This approach is still unexplored in homogenous molecular electrocatalysis, where inert cathode materials such as graphite and carbon nanoparticles are usually employed without any molecular modification. Furthermore, as the catalyst is in this case dissolved in solution, the system also differs from previous studies using heterogeneous CO_2RR catalysts in which the catalytically active sites, namely the metal atoms (Ag[19–21], Cu[22–28]), are part of the electrode and their activity is tuned by the presence of organic molecules, including imidazolium, immobilized on their surfaces. This is also different from imidazolium immobilization on polymer backbones for conducting membranes[29,30]. We also report here further scale up of the process by embedding positively charged imidazolium molecules on a metal-free gas diffusion electrode (GDE) surface (**Figure 1d**) and studying its impact on the performance of CO_2RR to formate catalyzed by complex **1** in acidic aqueous solution, which avoids carbon loss by carbonate formation, using a flow cell type reactor and an electrode of 10 cm^2 geometrical area (**Figures S1a** and **S1b**).

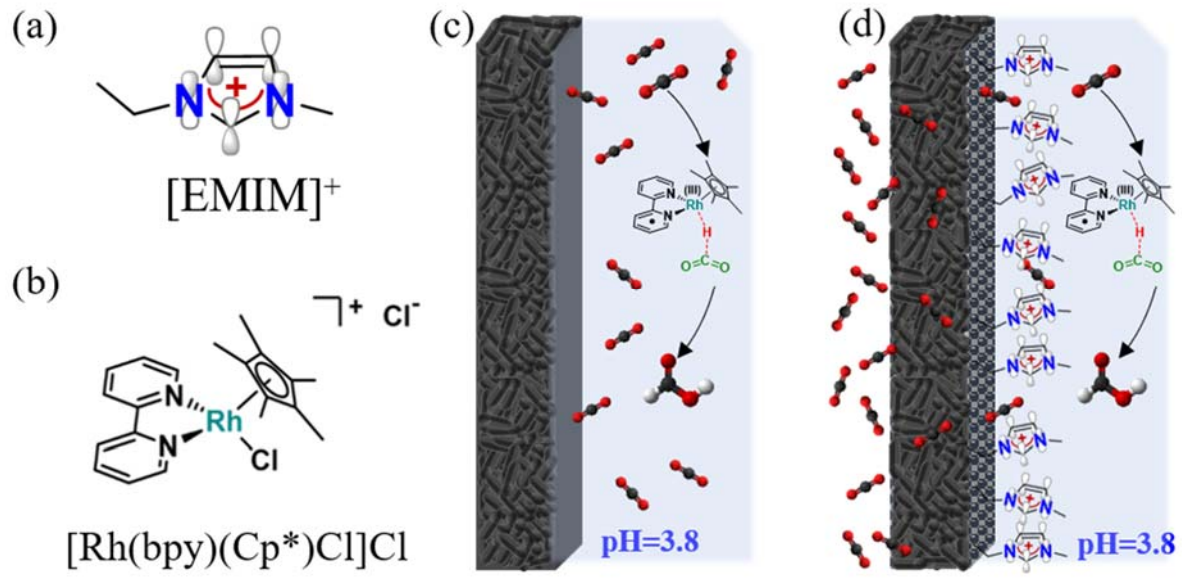

Figure 1. (a) $[EMIM]^+$ structure and (b) Rh complex **1** structure. Schematic representation of: (c) the mediated CO_2 conversion to formate on a bare glassy carbon (GC) electrode in a liquid-phase electrolyzer, (d) mediated CO_2RR on a GDE modified by a layer of $[EMIM]^+$ in a gas-phase electrolyzer.

EXPERIMENTAL SECTION

Reactants. Anhydrous acetonitrile of 99.99% purity (CH_3CN), sodium acetate ($CH_3COONa{\cdot}3H_2O$ > 99%), tetrabutyl ammonium hexafluorophosphate ($[TBA][PF_6]$, > 99%), tetrabutyl ammonium tetrafluoroborate ($[TBA][BF_4]$, > 99%), 2,2′-Bipyridyl of ≥ 99% purity, dopamine hydrochloride of 98% purity and 2-Bromoethylamine hydrobromide of 99% purity were all purchased from Sigma-Aldrich. Acetic acid (CH_3COOH > 99.5%) was purchased from TCI chemicals. Rh Complex precursor dichloro(pentamethylcyclopentadienyl)rhodium(III) dimer $[Rh(Cp^*)Cl_2]_2$, of 99% purity was purchased from Strem Chemicals. Imidazolium salts: 1-ethyl-3-methylimidazolium hexafluorophosphate ($[EMIM][PF_6]$) (99%), 1-ethyl-3-methylimidazolium tetrafluoroborate ($[EMIM][BF_4]$) (either >98% or > 99%), 1-Butyl-3-methylimidazolium hexafluorophosphate ($[BMIM][PF_6]$) (99%), 1-Ethyl-2,3-dimethylimidazolium hexafluorophosphate ($[EDMIM][PF_6]$) (99%) and 1-ethyl-imidazole (> 98%) were all purchased from Io-li-tec (Germany). Ferrocene (98%) was purchased from Merck. All reactants were used without any further purification. All aqueous solutions were prepared with ultrapure water (18.2 MΩ cm, Millipore).

Synthesis of complex [Rh(bpy)(Cp*)Cl]Cl·H_2O. The following synthesis was adapted from existing protocols in the literature[31,32]. A methanol solution (30 mL) of 1 equivalent $[Rh(Cp^*)Cl_2]_2$ (200 mg, 0.32 mmol) and 2 equivalents 2 2'-bipyridine (120 mg, 0.76 mmol) was stirred at RT for 2 h in the dark. The resulting clear orange-yellow solution was evaporated until dry. The yellow solid was dissolved in a minimal quantity of acetonitrile (CH_3CN) and precipitated upon the addition of ethyl acetate (AcOEt), then collected on a Buchner funnel and dried under vacuum. The purity of the final precipitate was verified by ^1H NMR spectroscopy according to the literature[32]. **Figure S2** shows the ^1H NMR spectrum of [Rh(bpy)(Cp*)Cl] (300 MHz, CD_3CN): δ/ppm, 1.61 (s, 15H), 7.71 (ψt, J = 7.2 Hz, 2H), 8.13 (dt, J = 7.7 Hz, 2H), 8.30 (d, J = 8.0 Hz, 2H), 8.78 (d, J = 5.5 Hz, 2H).

Imidazolium immobilization and electrochemical characterization. All electrochemical experiments were performed either on SP-300 or VSP-300 potentiostats/galvanostats (Bio-Logic Science Instruments SAS) and were conducted at room temperature (20 ± 2 °C) in different solvents (CH_3CN, H_2O and mixtures of both of them). Either [TBA][PF_6], [TBA][BF_4], [EMIM][PF_6] or [EMIM][BF_4] were used as a supporting electrolyte in solution (0.5 M). Ar (> 99.99%) and CO_2 (> 99.99%) gases used to saturate solutions were purchased from Air Liquide.

i) Synthesis of imidazolium-based layers on carbon-based electrodes:

i.1.) Grafting imidazolium (IM^+) derivatives by an electrochemical-chemical (EC) two steps covalent method (IM^+_{EC}). This synthesis on the GC disc or plate (Alfa Aesar) surface was performed following a well-documented procedure from the literature[33]. It involves two reaction steps: *1*) the electrochemical grafting of the initiator layer, which is obtained by 5 consecutive cyclic voltammograms from 0 V to 1.6 V vs. Ag/AgCl/KCl_{sat} in an Ar saturated aqueous solution containing 1 mM 2-bromoethylamine and 0.1 M KCl, which leads to the attachment of the amine-based molecule on the electrode surface bearing a Br end group available and *2*) a chemical step, which comprises the nucleophilic substitution between the Br on the initiator layer and an imidazole derivate (1-ethyl-imidazole) dissolved in acetonitrile solution heated at 50 ºC overnight. The resulting IM^+_{EC} electrode is sketched in **Figure S3c.**

i.2) Grafting imidazolium (IM^+) derivatives by an electrochemical-electrochemical (EE) two steps covalent method (IM^+_{EE}). This synthesis was carried out successfully on three different carbon-based electrodes: A GC disc or plate (Alfa Aesar), a 3-dimensional reticulated vitreous carbon (RVC) foam (ERG Materials and Aerospace Co.) and a carbon-based gas diffusion electrode (GDE), Sigracet 28 BC (Fuel Cell Store). It involves two reactions steps:

1) Electrochemical reduction of $[EMIM]^+$ to form an imidazole layer at the carbon electrode as was described by Y. Wang and coworkers[34] on Cu electrodes and *2*) subsequent electrochemical oxidation at open circuit potential to form the positively charged imidazolium layer, as described in **Figure S3b and S4.** This imidazolium-based layer can be synthesized either in aqueous or acetonitrile solution*:*

i.2.1) Synthesis and optimization of IM^+_{EE} in acetonitrile solution: The synthesis of IM^+_{EE} was optimized on a GC disc by studying the following parameters: type of electrochemical deposition technique (cyclic voltammetry (CV) or chronoamperometry (CA)), the potential window scanned by CV, the duration of electrodeposition by CA (from 10 s to 15 min), the IL concentration in solution (from 0.01 to 1 M), the chemical composition of imidazolium-based IL with either different cations or anions and in the presence or absence of CO_2 in solution. The impact of each varied parameter on the modified carbon electrode was evaluated by CV of complex **1** under catalytic conditions (**Figures S5-S10**). Thus, the optimal conditions of IM^+_{EE} synthesis were CA in an Ar saturated 0.5 M $[EMIM][PF_6]$ or $[EMIM][BF_4]$ acetonitrile solution at -3.95 V vs Fc^+/Fc for 10 s. During the second step, the electrode rested in solution at open circuit potential (OCP) -0.4 V vs Fc^+/Fc for approximately 10 min to totally complete the oxidation step. Afterwards, this electrode was removed from the cell, rinsed with acetonitrile and placed in a new solution for its subsequent characterization and catalytic evaluation. A Pt wire was used as a counter electrode and an all solid Ag/AgCl wire directly immersed in acetonitrile solution was used as pseudo-reference electrode. Additionally, ferrocenium/ferrocene (Fc^+/Fc) redox couple was added in solution as an internal reference. *i.2.2) Synthesis of IM^+_{EE} in aqueous solution*: The synthesis of IM^+_{EE} on carbon-GDE and RVC electrodes took place by CA in an Ar saturated 0.5 M $[EMIM][BF_4]$ aqueous solution at -2.5 V vs $Ag/AgCl/KCl_{sat}$ for 10 s. The second step for the synthesis of IM^+_{EE} comprises the electrode resting in solution at open circuit potential (OCP) -0.1 V vs $Ag/AgCl/KCl_{sat}$ for approximately 10 min. Afterwards, this electrode was removed from the cell, rinsed with water and placed in a new solution for its subsequent catalytic evaluation. For that purpose, a 5 cm^2 GC rod (Alfa Aesar) as a counter electrode and $Ag/AgCl/KCl_{sat}$ electrode within a salt bridge as a reference electrode were used.

ii) Electrochemical characterization of IM^+_{EE} and IM^+_{EC} modified electrodes in the presence of different molecular probes by cyclic voltammetry.

CV experiments were carried out in a three-electrodes setup, with a GC disc electrode (0.07 cm^2) where either IM^+_{EE} or IM^+_{EC} were previously deposited as a working electrode (BioLogic). A platinum wire was used as a counter electrode (diameter = 0.5 mm, Alfa Aesar, 99.5% purity) and was previously flame annealed. The reference electrode used in all cases was a conventional $Ag/AgCl/KCl_{sat}$ reference electrode (BioLogic) separated from the solution by a salt bridge. In acetonitrile however, all potentials were calibrated using the ferrocenium/ferrocene (Fc^+/Fc) redox couple as an internal standard, which was added in the solution at the end of each experiment. CVs were run at either 0.1 or 0.01 V s^{-1} scan rate and only the third steady state cycle of all CVs is shown, unless otherwise stated in the text. Dopamine, ferrocene and acetic acid were used as molecular redox probes in solution. Moreover, catalytic activity for CO_2RR catalyzed by the Rh complex **1** was also evaluated on both IM^+_{EE} and IM^+_{EC} cathodes.

Surface characterization techniques. The Scanning Electron Microscopy and Energy-Dispersive X-ray Spectroscopy (SEM-EDX) analysis were performed in an Ultra 55 ZEISS microscope equipped with a spectrometer Quantax from Bruker (**Figure S11**). The binding energy was calibrated using a Cu disk. IM^+_{EC} and IM^+_{EE} samples were sonicated for 5 minutes, dried and carbon coated (5-10 nm) to ensure high conductivity of the sample before SEM analysis. Water contact angle (WCA) was quantified using Drop Shape Analyzer - DSA25 from KRÜSS. Attenuated total reflection Fourier transform infrared (ATR-FTIR) spectroscopy was performed using a Bruker VERTEX 70 FTIR spectrometer utilizing diamond ATR accessory (Quest™, Specac). Measurements of dry solid samples were carried out at room temperature in ATR mode. The spectra were acquired from 650 to 4000 cm^{-1} with a spectral resolution of 4 cm^{-1}, and a total of 100 scans were recorded for each spectrum. The spectra were normalized by baseline correction, water signal subtraction and smoothing. X-Ray Photoelectron Spectroscopy (XPS) spectra of IM^+_{EC} and IM^+_{EE} were collected on gold electrodes using a Omicron Argus X-ray photoelectron spectrometer, equipped with a monochromated AlKα radiation source (hν = 1486.6 eV) and a 280 W electron beam power. The diameter of analyzed area was 1 mm^2. The emission of photoelectrons from the sample was analyzed at a takeoff angle of 45° under ultra-high vacuum conditions ($\leq 10^{-9}$ mBar). Survey spectra were carried out with a 100 eV pass energy and 20 eV pass energy was used for the high resolution C 1s and N 1s spectra. Binding energies were calibrated against the C 1s (C-C) binding energy at 284.8 eV and element peak intensities were corrected by Scofield factors. The peak areas were determined after subtraction of a linear background. The spectra were fitted using Casa XPS v.2.3.15 software (Casa Software Ltd, U.K.) and applying a Gaussian/Lorentzian ratio (G/L) equal to 70/30.

CO_2 conversion by constant current electrolysis. *i*) CO_2 saturated solution recirculation in a two-compartments H-type cell. Catalytic activity evaluation of the Rh molecular catalyst for CO_2RR by electrolysis at constant current density applied of -3.33 mA cm^{-2} was performed in a gastight two-compartments electrochemical H-type glass cell with a glass frit separating anolyte (5 mL) and catholyte (10 mL) solutions. Electrolysis were performed in acetonitrile solution containing between 5% and 50% v/v H_2O or in purely aqueous solutions, together with 0.5 M of supporting electrolyte ([TBA][PF_6], [TBA][BF_4] or [EMIM][PF_6]) previously saturated with CO_2 by gas bubbling in both catholyte and anolyte, but no continuous CO_2 gas was purged during the electrolysis. 1 mM of Rh complex was only added in the catholyte and 0.1 M CH_3COO^-/CH_3COOH buffer solution (pH = 3.8) was also added as additional supporting electrolyte in purely aqueous solutions. The working electrode was: 1) In acetonitrile solutions, a 1 cm^2 GC plate (1 mm thick, type 2, from Alfa Aesar) with (IM^+_{EE} and IM^+_{EC}) or without (pristine GC) grafted imidazolium on their surface. 2) In purely aqueous solution, a 3-dimensional reticulated vitreous carbon (RVC) foam (geometrical area = 3 cm^2 and pores per inch (PPI) = 45) Duocel® from ERG Materials and Aerospace Co, with (IM^+_{EE} and IM^+_{EC}) or without (pristine RVC) grafted imidazolium on their surface. In all cases, the counter electrode was a 5 cm^2 GC rod (Alfa Aesar), the current density (3.33 mA cm^{-2}) was calculated using the cathode geometrical area and the evolution of the cathode potential during the electrolysis was measured with respect to an $Ag/AgCl/KCl_{sat}$ reference electrode located within a double bridge. Constant current electrolysis lasted for 15 C in acetonitrile solutions and 10 C in aqueous solutions. All electrolysis experiments were performed with 2 or 3 replicates to check results reproducibility. *ii*) CO_2 gas-phase electrolysis in flow cell type reactor. Catalytic activity evaluation in aqueous solution of the Rh molecular catalyst for CO_2RR by large scale electrolysis in a two compartments flow cell type reactor is described in **Figure S1**. Constant current density applied = (20 - 100 mA cm^{-2}). Catholyte composition in flow: 1 mM Rh complex, 0.1 M [TBA][BF_4] and 0.1 M CH_3COO^-/CH_3COOH buffer (pH = 3.8) aqueous solution. Anolyte composition with recirculation: 0.5 M KOH aqueous solution. Humidified CO_2 gas fed into the GDE at a flow rate of 190 mL min^{-1}. The flow cell type reactor and all associated parts, such as end frames, endplates, Teflon flow frames, PVDF turbulence mesh, gaskets and hardware for cell assembly were all purchased from ElectroCell Europe A/S (Denmark). The cathode used was a carbon-based gas diffusion electrode (GDE), Sigracet 28 BC purchased from Fuel Cell Store (USA) with a geometric area of 10 cm^2, which contains a hydrophobized gas diffusion layer (5 wt.% PTFE) and a microporous carbon layer. This GDE was used with or without $[EMIM]^+$ on its surface (IM^+_{EE}). In particular, IM^+_{EE} was

electrochemically deposited by chronoamperometry of 10 s from a 0.5 M [EMIM][BF_4] aqueous solution following the previously described protocol of synthesis. The anode was a Dimensionally Stable Anode (DSA) electrode, made from an IrO_2–Ta_2O_5 mixed oxide and the ionic membrane separating both compartments was a Nafion 117 membrane (183 μm thickness), both purchased from ElectroCell Europe A/S (Denmark). Finally, all tubing used to link the flow electrolyzer with the solution reservoirs were C-Flex Ultra 14 (Internal Diameter (ID) = 1.6 mm), purchased from Cole-Parmer. Catholyte/anolyte recipients were glass bottles of 100 mL, purchased from Dewar and catholyte flow rate was 1.1 mL min^{-1}. The reactor configuration used for all experiments shown was a single-pass flow configuration for both catholyte and CO_2 and recirculation for the anolyte. The solution pH in both anolyte and catholyte was measured at the end of each electrolysis and no significant difference from the initial pH was reported. The peristatic pump used to feed the flow cell type reactor with the electrolyte solution was the Master Flex L/S model Easy Load II from Cole Parmer. The DC power supply used to apply a constant current during the electrolysis also measured simultaneously the cell potential and it was the model IT6874A from ITECH (1 A/150 V or 2 A/60 V).

Analytical quantification of products and figures of merit. Gas products were quantified by gas chromatography (Model 8610C SRI Instruments) equipped with TCD and FID detectors from 50 μL aliquots of the headspace of both compartments. Only hydrogen (H_2) was detected as a gas product. Liquid products were evaluated using an ionic exchange chromatograph (IC) (Metrohm 883 Basic IC) equipped with a Metrosep A Supp 5 column and a conductivity detector. Only formate was detected. A typical quantification of formate by IC required the sampling of 50 μL of solution from catholyte and/or anolyte, followed by a (200 - 400) dilution in ultrapure water and a final injection of 20 μL into the IC chromatograph. Figures of merit evaluated are: Faraday efficiency (FE, %) of each reaction product (FE_{HCOO^-} and FE_{H2}), the cathodic half reaction energy efficiency (EE_{HCOO^-}, %), the full cell energy efficiency ($EE_{full\ cell}$, %), the production rate (r) (g m^{-2} min^{-1}) of CO_2RR reaction product (r_{HCOO^-}) and the energy consumption (EC, kWh $kmol^{-1}$) to produce the target product (formate). All figures of merit calculation is described in the supporting information content.

RESULTS

Briefly, the two strategies for immobilization of positively charged imidazolium molecules at the electrode surface studied here are (**Figure S3**): *i*) (IM^+_{EC}), a two-steps electrochemical-

chemical (EC) method for covalent grafting of imidazolium (IM^+) derivatives[33] based on grafting first a haloamine onto the electrode, followed by nucleophilic substitution by an imidazole derivative and *ii*) (IM^+_{EE}), a new two-steps electrochemical-electrochemical method for covalent grafting of imidazolium derivatives, based on, first, the electrochemical reduction of $[EMIM]^+$ to form an imidazole layer at the carbon electrode as described by Y. Wang and coworkers[34] on Cu electrodes and then, electrochemical oxidation at open circuit potential to form the positively charged imidazolium layer (**Figure S4**). **Figure 2** shows some morphological, physical, chemical and spectroscopic characterization of the pristine glassy carbon (GC) cathode (**Figure 2a**) and the modified GC cathodes obtained by imidazolium cation immobilization (IM^+_{EE} and IM^+_{EC}). Both imidazolium-based layers are water- and acetonitrile-insoluble. SEM images of IM^+_{EE} and IM^+_{EC} optimal cathodes show the presence of a thin layer deposited on top of the GC substrate, (**Figure 2b** and **2c**, respectively), but the layer is incompletely covering the surface. Additional SEM images and energy dispersive X-ray (EDX) analysis comparing GC and IM^+_{EE} cathodes (**Figure S11**) provide chemical composition information and prove the presence of imidazolium cations immobilized on the electrode surface together with their corresponding counter anion (PF_6^-). Interestingly, the surface wettability measured by water contact angle (WCA) significantly shifts from a slightly hydrophobic surface in pristine GC cathode (86º, **Figure 2d**) to a highly hydrophilic cathode surface in IM^+_{EC} (25º, **Figure 2f**) and an extremely hydrophilic surface in IM^+_{EE} (3º, **Figure 2e**). It seems to indicate a different density of imidazolium at the electrode surface depending on immobilization strategies (IM^+_{EE} and IM^+_{EC}) and reveals a gain in wettability on both modified electrodes by the formation of a charged-surface, which is much more polar and hydrophilic than the bare GC. In contrast, the synthesis of the IM^+_{EE} using larger reaction times (15 min) than those chosen as optimal (10 s), as well as using other imidazolium-based ILs as a precursor ($[EDMIM][PF_6]$) generated a more hydrophobic layer on the electrode surface with a higher WCA value (40-50º).

The attenuated total reflection Fourier transform infrared (ATR-FTIR) spectra of the IM^+_{EE} and IM^+_{EC} cathodes are similar and almost superimposable in the region of >2000 cm^{-1} with that of the pure $[EMIM][BF_4]$ spectrum, suggesting, in both cases, a structure of the molecular component of the layer similar to that of $[EMIM][BF_4]$ (**Figure 2g**). In particular, the bands marked by a dotted line at 3162 cm^{-1} (C_4-H and C_5-H stretching) and 3122 cm^{-1} (C_2-H stretching), which are associated with the vibrations of the C-H bonds within the aromatic ring[35,36], are identical (zoom in **Figure 2h**). This means that all three C-H bonds initially present in the aromatic ring of $[EMIM]^+$ are conserved after the immobilization of imidazolium onto

the electrode. Other characteristic bands that remain unchanged in all three ATR-FTIR spectra are shown at 1570 cm^{-1}, attributed to the C=C stretching, 1171 cm^{-1}, assigned to the stretching of the methyl-N and ethyl-N bonds, as well as 1017 cm^{-1} associated with the BF_4^-counter anion[35,36]. Those bands are also marked by a dotted line within **Figure 2g**. Nevertheless, a new band at 1635 cm^{-1} (marked with * in **Figure 2g**) appears in both IM^+_{EE} and IM^+_{EC} cathodes spectra. This band is very likely attributed to the H-O-H bending mode of water molecules trapped in the imidazolium ad-layer next to the electrode[11,36,37]. Moreover, this low wavelength band is related to the OH-stretching band at 3610 cm^{-1}, which is consistent with previous studies[36] (**Figure S12**). Finally, IM^+_{EC} cathode spectrum presents three additional bands, the first one at 1054 cm^{-1} attributed to the secondary aliphatic amines stretching mode (C-N stretching or C-N elongation vibration), the other two bands, at 840 cm^{-1} and 746 cm^{-1}, associated with C-Cl and C-Br elongation vibration modes, respectively and due to an incomplete imidazolium functionalization of the electrode. Indeed, the initial electrochemical step for preparation of IM^+_{EC} leads to the immobilization of bromo-ethylamine at the electrode surface. Thus, the presence of a C-Br band at 746 cm^{-1} indicates that the terminal Br group is not completely replaced by imidazolium all over the surface. Moreover, Br can be partly exchanged with Cl^- from KCl solution, as indicated by the presence of C-Cl band at 840 cm^{-1}. In conclusion, a mixture of different immobilized molecules is obtained at the electrode surface in the case of IM^+_{EC}, as is sketched in **Figure S3c**.

The XPS analysis of two IM^+_{EE} cathodes synthesized either in acetonitrile or in aqueous solution, as well as of the IM^+_{EC} cathode, was also performed on gold electrode instead of GC for improving the signal-to-noise ratio in analyzing elemental carbon. For this reason, the survey XPS spectra for IM^+_{EE} and IM^+_{EC} cathodes shown in **Figure S13** exhibit the Au signal besides confirming the coexistence of C, N and O elements on all three cathode surfaces. Moreover, **Figure S13** proves that the composition of IM^+_{EE} is solvent independent, since the XPS survey is the same whether the material was deposited in acetonitrile or in water. **Figure 2i** shows the N1s core level spectra of the IM^+_{EE} and IM^+_{EE} cathodes. Three contributions can be de-convoluted in both spectra, with the main contribution at 400.1 ±0.1 eV being assigned to metal-bound N[28,38,39], the second peak at 398.7±0.1 eV assigned to pyridinic N, and a peak at higher binding energies, 401.7 ±0.1 eV, which can be assigned either to pyrrolic N or quaternary (N^+)[40,41]. Overall, the XPS spectra corroborate the presence of a layer containing imidazolium moieties immobilized on the electrode surface in both cases.

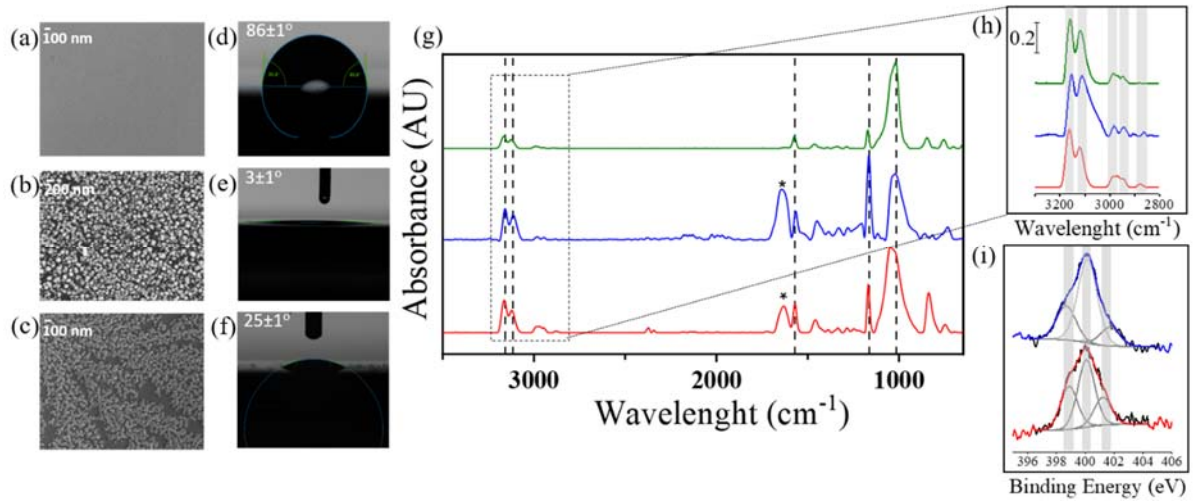

Figure 2. Morphological and chemical characterization by SEM and WCA of the pristine GC cathode (2a and 2d) and the modified GC cathodes obtained by imidazolium cation immobilization, named IM^{+}_{EE} (2b and 2e) and IM^{+}_{EC} (2c and 2f). Spectroscopic characterization of the same cathodes by ATR-FTIR (2g and 2h (zoom of 3000 cm^{-1} region)) and the modified GC cathodes by XPS high-resolution spectra for N (1s) (2i). Green plots correspond to GC cathode with a drop of [EMIM][BF_4] on top, blue plots correspond to IM^{+}_{EE} cathode and red plots correspond to IM^{+}_{EC} cathode. IM^{+}_{EE} cathode synthesized in 0.5 M [EMIM][BF_4] acetonitrile solution.

Electrochemical characterization by cyclic voltammetry of the surface-charged IM^{+}_{EE} cathode confirms the presence of an immobilized molecular layer on the electrode surface (**Figure S14**). In particular, the anodic peak at -0.9 V *vs.* Fc^{+}/Fc during the synthesis of IM^{+}_{EE} (**Figure S4**) is only present if the cathodic potential is scanned down to E<-2.45 V *vs.* Fc^{+}/Fc (black plot in **Figure S14a**). This is in agreement with previous reports studying the electrochemical stability of pure imidazolium-based ionic liquids[42–45]. In contrast, this oxidation peak is no longer present if the lowest cathodic potential is limited to E>-2.45 V *vs.* Fc^{+}/Fc, too positive to allow reduction of imidazolium (red plot in **Figure S14a**). The nature of this oxidation process is demonstrated to be adsorption- and not diffusion-controlled based on the linear relationship established between the oxidation current density at the peak potential (j_p^{ox}) and the potential scan rate[46] (**Figures S14b** and **S14c**). Additional electrochemical characterization of surface-modified electrodes, such as IM^{+}_{EE} and IM^{+}_{EC} cathodes, is achieved by studying the behavior of different electroactive molecular probes in solution. In particular, the electrochemical response of a molecular probe is controlled by the type of reactions taking place at the surface-

modified electrode, outer- or inner-sphere reactions, which are either mainly insensitive or strongly dependent on the nature of the electrode surface, respectively[47]. **Figure 3** shows the electrochemical response of pristine GC, IM^{+}_{EE} and IM^{+}_{EC} electrodes for three different molecular redox probes, dopamine, proton and ferrocene, two inner- and one outer-sphere redox probes, respectively. **Figure 3a** shows the redox behavior of dopamine in acidic aqueous solution on the three electrodes. In the case of IM^{+}_{EE} (blue plot) and IM^{+}_{EC} (red plot) electrodes an increase in the oxidation-to-reduction peak separation is observed (by a factor of 1.6 and 4) with respect to the pristine GC electrode (black plot), which is consistent with the presence of a molecular layer on IM^{+}_{EE} and IM^{+}_{EC} electrodes, since dopamine redox reaction becomes more irreversible there. **Figure 3b** shows the redox behavior of ferrocene in acetonitrile solution on the three electrodes as well. In this case, on both IM^{+}_{EE} (blue plot) and IM^{+}_{EC} (red plot) electrodes, the peak-to-peak separation is identical to that of the pristine GC electrode (black plot), which demonstrates that the presence of immobilized imidazolium on the electrode has no impact on its electron transfer resistance. **Figures 3c** and **3d** show the irreversible redox behavior of proton reduction in acetonitrile solution during HER on the three cathodes, either in the absence or the presence of Rh complex, respectively. In comparison with pristine GC electrode (black plot), a 4-5 fold diminution in current density and an increase in overpotential for HER are observed in the case of both IM^{+}_{EE} and IM^{+}_{EC} electrodes (blue and red plots, respectively), in agreement with a positively charged surface contributing to HER suppression. This fact is relevant here because HER is in competition with CO_2RR, and such a modification is likely to favor CO_2RR[18,48].

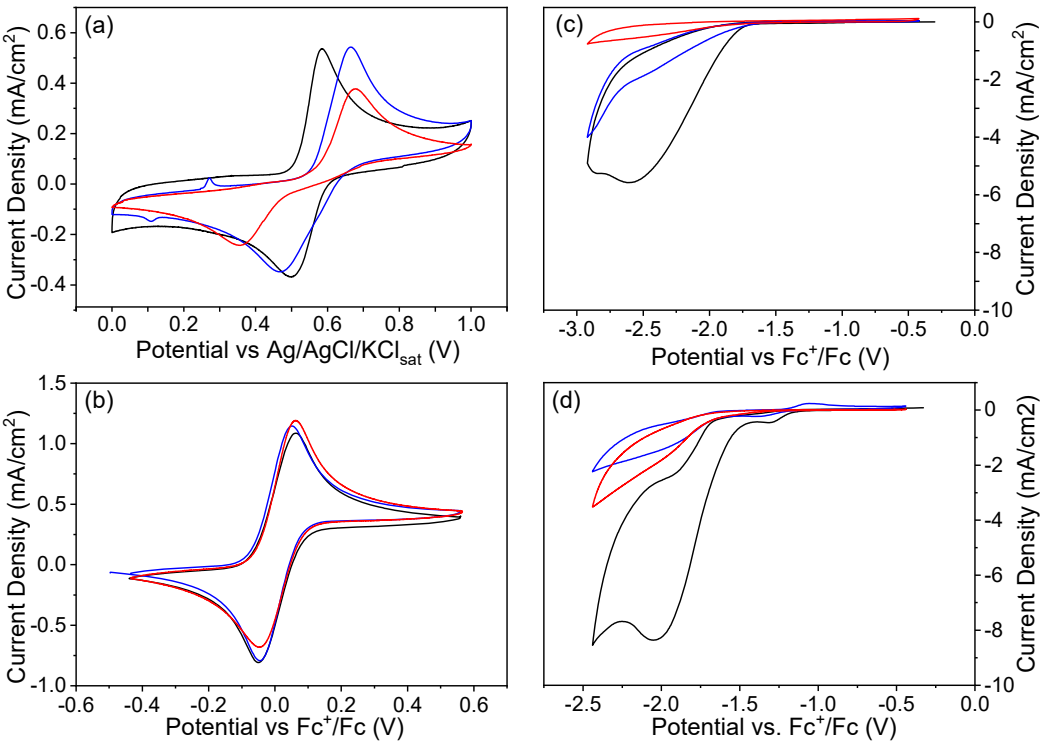

Figure 3. (a) CVs of 10^{-3} M dopamine in Ar saturated 0.1 M H_2SO_4 aqueous solution. (b) CVs of 5 x 10^{-3} M ferrocene in Ar saturated 0.1 M [TBA][PF_6] acetonitrile solution. (c) CVs of 0.1 M CH_3COOH in Ar saturated 0.5 M [TBA][PF_6] acetonitrile solution. (d) CVs of 10^{-3} M ([Rh(bpy)(Cp*)Cl]Cl in Ar saturated 0.1 M CH_3COOH and 0.1 M [TBA][PF_6] acetonitrile solution. Scan rate 0.1 V s^{-1}. Black plots correspond to pristine GC, blue plots to IM^+_{EE} and red plots to IM^+_{EC} cathodes.

CO_2RR activity catalyzed by the Rh complex **1** on pristine GC and modified (IM^+_{EE} and IM^+_{EC}) electrodes was studied by CV (**Figure 4a**) and bulk electrolysis in a H-type cell (**Figure 4b**). We have recently shown that the Rh complex is nicely suitable for this kind of study as it is very sensitive to variations in the electrode/electrolyte interface, in terms of catalytic onset potential and products selectivity (CO_2RR vs. HER)[18]. **Figure 4a** shows that both modified electrodes IM^+_{EE} (blue plot) and IM^+_{EC} (red plot) exhibit more anodic onset potentials (marked by dotted lines) and higher peak current densities for the CO_2RR catalytic wave as compared to pristine GC electrode (black plot) in the same electrolyte. Furthermore, CVs of all 3 electrodes in acetonitrile solution containing 0.5 M [TBA][PF_6] are compared with the one displayed by pristine GC cathode in an imidazolium-based IL acetonitrile solution (0.5 M [EMIM][PF_6], green plot) in **Figure 4a**. **Table S1** summarizes the onset potentials and the half-wave catalytic potentials ($E_{cat/2}$) from all 4 CVs presented in **Figure 4a**. Imidazolium modified electrodes (IM^+_{EE} and IM^+_{EC}) displace the onset potential (60-100 mV) and $E_{cat/2}$ (30-50 mV)

more anodic with respect to the pristine GC cathode with $[TBA]^+$ in solution. **Figure 4b** shows the faradaic efficiency (FE) of the two main products obtained (formate and H_2), as well as the cathodic half reaction energy efficiency for formate production (EE_{HCOO^-}) obtained from control current electrolysis at -3.33 mA/cm^2 during 77 min in a two-compartments H-type cell with Rh complex **1** in different electrolytes: CO_2-saturated acetonitrile (with either 5 or 50% water) or CO_2-saturated aqueous solution. Formic acid/formate was detected as the only product in the liquid phase and only H_2 was observed in the gas phase. **Figure S15** shows the cathode potential evolution as a function of constant current electrolysis time in acetonitrile with 5 and 50% (vol.) H_2O. The cathode potential is almost identical using either IM^+_{EE} (blue curve) or IM^+_{EC} (red curve) cathodes and pristine GC cathode with [EMIM][PF_6] as electrolyte in acetonitrile solution (green curve), furthermore almost 1 V lower than that obtained with pristine GC and a conventional electrolyte (black curve) (**Figure S15**). A significant, but smaller, shift in potential is also observed during CO_2RR in acetonitrile/water 50/50 v/v solutions (**Figure S15**). In aqueous solution, the cathode potential decreases during electrolysis resulting in a low overpotential for CO_2 conversion to formate at pH 3.8 on modified IM^+_{EE} cathode (blue curve) (< 0.4 V, **Figure S16**). Thus, **Figure 4b** shows that IM^+_{EE} and IM^+_{EC} modified cathodes provide a great improvement in catalytic performance in acetonitrile/H_2O 95/5 v/v solution on both parameters: FE_{HCOO^-} (85-81%) and EE_{HCOO^-} (59-58%) in comparison with pristine GC cathode (FE_{HCOO^-} 53% and EE_{HCOO^-} 24%). As expected, pristine GC cathode using [EMIM][PF_6] as the electrolyte results also in an increase of FE_{HCOO^-}, albeit to a minor extent (FE_{HCOO^-} 69% and EE_{HCOO^-} 47%). The same catalytic trend (IM^+_{EE} more active than bare GC) is observed from electrolysis results obtained by increasing the amount of water in solution (either 50 or 100%) (**Figure 4b**). In particular, CO_2RR in acidic aqueous solution (buffer solution at pH = 3.8) represents a suitable medium for large scale applications, since acidic solutions limit CO_2 losses due to carbonate and bicarbonate generation in alkaline and neutral aqueous solutions[14,18]. Thus, the data reported in **Figure 4b** and **Figure S16** show that IM^+_{EE} cathode works efficiently under acidic aqueous conditions at a very low overpotential, while keeping significant selectivity for formic acid production (FE_{HCOO^-} = 53% and EE_{HCOO^-} = 33%), thanks to its HER suppressing effect (FE_{H2} = 42% as compared to FE_{H2} = 58% for pristine GC cathode).

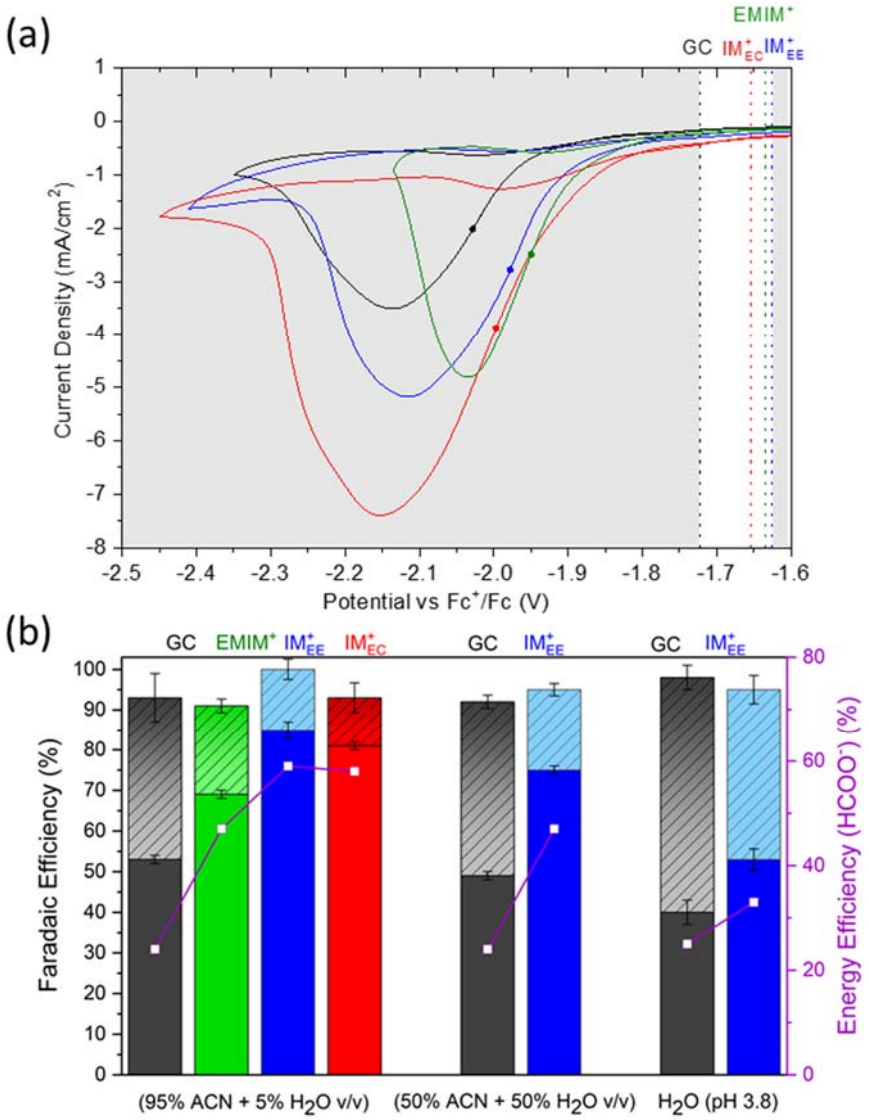

Figure 4. (a) CVs of 1 mM Rh complex on different cathodes in acetonitrile solution containing 5% v/v H_2O under CO_2 using 0.5 M [TBA][PF_6] or [EMIM][PF_6] (color code below). Scan rate 0.01 V s^{-1}. Vertical dotted line sets the onset potential and $E_{cat/2}$ is represented by a point in each CV (b) Faradaic efficiencies of formate (FE_{HCOO^-} ▭) and of hydrogen (FE_{H2} ▨), as well as energy efficiency (EE_{HCOO^-} ◘) from electrolysis of 1 mM Rh complex on different cathodes in 0.5 M of different electrolytes and CO_2 saturated solutions at -3.33 mA cm^{-2} in a two-compartments H-type cell. Black plot and bars: pristine GC cathode and 0.5 M [TBA][PF_6] in acetonitrile or [TBA][BF_4] in aqueous solution. Green plot and bar: pristine GC cathode and 0.5 M [EMIM][PF_6] in acetonitrile solution. Blue plot and bars: IM^+_{EE} cathode and 0.5 M [TBA][PF_6] in acetonitrile or [TBA][BF_4] in aqueous solution. Red plot and bar: IM^+_{EC} cathode and 0.5 M [TBA][PF_6] in acetonitrile solution.

Finally, we conducted additional efforts to scale up the CO_2 conversion process described here. For that purpose, we used a 10 cm^2 IM^+_{EE} cathode integrated into a flow cell type reactor (**Figures S1a** and **S1b**) allowing industrially relevant current densities to be achieved. **Figure S1c** shows a schematic representation of the scaled experimental setup for CO_2 conversion. In order to avoid mass transfer limitations imposed by CO_2 solubility in water, a carbon-based GDE directly fed with a flow of CO_2 gas from the backside[49] was used as a substrate for grafting imidazolium molecules by a 10 s chronoamperometry (IM^+_{EE}/GDE, **Figure 1d**) and compared to a blank cathode (bare GDE). The flowing catholyte was an acidic aqueous solution containing Rh complex **1**, acetate buffer and 0.1 M [TBA][BF_4], while the anolyte was a 0.5 M KOH recirculated solution. An initial electrochemical activation period, noted by a yellow square in **Figure 5a,** is necessary to increase the wettability of carbon-based GDEs before reaching a steady-state performance. This electro-wetting effect has been already described in the literature[50]. **Figure 5a** shows the results of the IM^+_{EE}/GDE cathode in terms of formic acid production rate for 9 consecutive, but discontinuous, electrolysis of 1000 C at different current densities (20, 50 and 100 mA cm^{-2}). The stable catalytic activity of the IM^+_{EE}/GDE cathode under operating conditions is demonstrated in **Figure 5a** from the slight increase in formate production rate (r_{HCOO^-} = 1.3 g_{HCOO^-} m^{-2} min^{-1}) reached after the activation period in 4 independent electrolysis at 20 mA cm^{-2} using the same electrode (electrolysis from 4 to 7 in **Figure 5a**). **Figure S17** displays the cell potential (E_{cell}) in the flow cell reactor as a function of total circulated charge corresponding to the first 7 consecutive electrolysis shown in **Figure 5a**. **Figure S17** shows a continuous decrease in E_{cell} by accumulating circulated charge during CO_2 conversion, which fits with a stable IM^+_{EE}/GDE cathode. In contrast, the performance of the bare carbon GDE cathode after the activation period at 20 mA cm^{-2} under the same operating conditions is 25% smaller (r_{HCOO^-} = 0.9 g_{HCOO^-} m^{-2} min^{-1}, electrolysis 4 in **Figure S18a**). A greater impact in formate production rate (+62%) is observed at 50 mA cm^{-2} for the same amount of charge circulated (8000 C) by comparing IM^+_{EE}/GDE (3.4 g_{HCOO^-} m^{-2} min^{-1}, electrolysis 8 in **Figure 5a**) and bare carbon GDE cathodes (2.1 g_{HCOO^-} m^{-2} min^{-1}, electrolysis 2 in **Figure S18b**). A maximum in r_{HCOO^-} on IM^+_{EE}/GDE cathode of 4.6 g_{HCOO^-} m^{-2} min^{-1} is reached at 100 mA cm^{-2} after 9000 C circulated on the same electrode (electrolysis 9 in **Figure 5a**). This applied current density is beyond the maximum that the bare carbon GDE cathode can handle before collapsing. **Figure 5b** shows energy consumption (EC) and full cell energy efficiency ($EE_{full\ cell}$) values obtained on both IM^+_{EE}/GDE and bare carbon GDE cathodes as a function of applied current density. Interestingly, the EC value obtained on the bare carbon GDE cathode sharply diminishes to half of its initial value on IM^+_{EE}/GDE cathode, from 1089

to 574 kWh kmol^{-1} at 20 mA cm^{-2} and from 1898 to 818 kWh kmol^{-1} at 50 mA cm^{-2} (red squares in **Figure 5b**). In parallel, the $EE_{full\ cell}$ value doubles by reaching a maximum of 8% at 20 mA cm^{-2} (bars graph in **Figure 5b**). These effects are due to the simultaneous enhancement in reaction selectivity (CO_2RR *vs*. HER) and diminution in overpotential achieved by modifying the carbon-based GDE with imidazolium on its surface. The stability of the IM^+ modification layer on the electrode was also evaluated using microscopy and spectroscopy. On the one hand, IM^+_{EE}/GDEs were characterized by EDX after the activation period (**Figure S19**) and SEM after 9 consecutive CO_2RR electrolysis (**Figure S20**). No significant change could be observed as compared to the initial material. Those results demonstrate that the IM^+ layer on the GDE remains attached to the electrode surface after both activation and long-term electrolysis. On the other hand, XPS characterization of the modified electrodes after CO_2 electrolysis in H-type cell was also performed (**Figure S21**) and clearly showed the presence of the N signal associated with the imidazolium immobilized at the electrode surface.

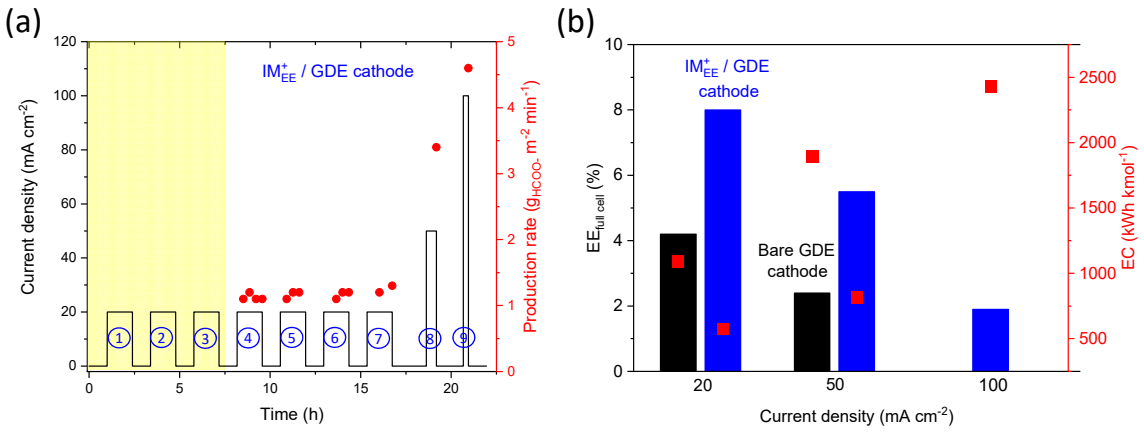

Figure 5. CO_2 gas-phase electrolysis results in a flow cell type reactor using 1 mM Rh complex **1** in acidic aqueous solution (pH 3.8). (a) Nine consecutive electrolysis of 1000 C each performed at different current densities (electrolysis from 1 to 7 at – 20, electrolysis 8 at -50 and electrolysis 9 at -100 mA cm^{-2}) on an IM^+_{EE}/GDE cathode. The yellow zone represents the initial electrochemical activation period of the cathode. (b) Average full cell energy efficiency (bars plot) and energy consumption (red squares plot) for formate production as a function of applied current density on a bare carbon GDE (black column) and IM^+_{EE}/GDE (blue column), respectively.

DISCUSSION

In order to evaluate the potential of tuning LEFs at the surface of carbon electrodes to optimize CO_2RR catalyzed by a molecular complex, we have used an imidazolium precursor, namely [EMIM][PF_6] or [EMIM][BF_4], to deposit a positively charged organic layer of $[EMIM]^+$ on the surface of a GC cathode. Two different immobilization methods have been used for generating the so-called IM^+_{EE} and IM^+_{EC} cathodes. The method leading to IM^+_{EE} is novel for immobilizing imidazolium on a carbon electrode and was optimized in this work. Those two cathodes have almost the same characteristics, indicating that a very similar material is generated in both cases. A broad combination of physicochemical methods has been used to characterize that deposited layer. In particular, SEM has unambiguously shown the presence of a solid material on the GC electrode (**Figure 2**). All chemical atoms initially present on the precursor [EMIM][PF_6] are also present on the deposited layer as shown by EDX (**Figure S11**) and XPS analysis (**Figure S13**). Moreover, the main contribution in the N1s XPS spectra displayed at 400 eV suggests N atom adsorbed on the surface (**Figure 2**). The presence of $[EMIM]^+$ molecules attached on the GC surface is further confirmed by the very characteristic ATR-FTIR spectrum of the material, which is almost superimposable with that of liquid $[EMIM]^+$ (**Figure 2**). All these results suggest a molecular-surface coupling through the N atom in both cases, IM^+_{EE} and IM^+_{EC} cathodes. Additional evidences are provided pointing to the presence of positive charges on the deposited material, as in the imidazolium cation used as precursor $[EMIM]^+$. Firstly, we observed a drastically shift in the WCA values (**Figure 2**) reflecting an increased hydrophilicity of IM^+_{EE} and IM^+_{EC} cathodes surfaces as compared to pristine GC. Secondly, electrochemical characterization through inner-sphere probe molecules such as dopamine and protons (**Figure 3**) confirmed the immobilization of imidazolium at the electrode surface and partial suppression of HER on both IM^+_{EE} and IM^+_{EC} cathodes. Thus, two different methods for imidazolium cation immobilization have been successfully used and the generation of a molecular charged-surface at the GC electrode has been demonstrated. The LEF generated at the electrode/electrolyte interface by the positively charged electrode surface might control the orientation, geometry and bond-dissociation energy of polarizable reactants, intermediates and/or products in electrochemical reactions. In particular, the impact of LEFs induced by a positively charged surface carbon-based electrode on activity and selectivity of CO_2RR catalyzed by molecular Rh complex **1** has been evaluated by CV and bulk electrolysis in different solvents (**Figure 4**). Firstly, much lower onset potential (up to 100 mV shift) and higher current density (up to double) for CO_2RR were obtained by CV after surface

modification on the GC electrode in **Figure 4a**. Comparable effects on the onset potential were observed with the bare GC cathode in 0.5 M [EMIM][PF_6] acetonitrile solution (**Figure 4a**), meanwhile lower catalytic current densities could be obtained in that case. Secondly, much larger selectivity for formate (*vs* H_2) production was obtained during electrolysis on charged surface electrodes as compared to bare GC cathode both in organic and aqueous solutions, with FE_{HCOO^-} reaching a value close to 90%, among the highest reported values for this catalyst so far. In pure aqueous solution, under acidic pH conditions, which greatly favors HER, FE_{HCOO^-} nevertheless reached 53% using the IM^+_{EE} cathode (**Figure 4b**). As a consequence, the combination of lower overpotentials and enhanced FE_{HCOO^-} with the IM^+_{EE} cathode results into an EE_{HCOO^-} value as high as 59% in acetonitrile solution with 5% v/v H_2O, 47% in acetonitrile solution with 50% v/v H_2O and 33% in purely aqueous solution (violet squares in **Figure 4b**). In contrast, the EE_{HCOO^-} value obtained by the bare GC cathode is solvent-independent (24% in all cases, **Figure 4b**). This value was increased in acetonitrile solution with 5% v/v H_2O (green bar in **Figure 4b**) only in the presence of [EMIM][PF_6] as the electrolyte (EE_{HCOO^-} = 47%), however without reaching the high values obtained with IM^+_{EE} and IM^+_{EC} cathodes.

Previous detailed DFT calculations[18] have provided a clear mechanistic understanding of the role of $EMIM^+$ as electrolyte in solution on the performance of the same molecular Rh complex **1** catalyst for CO_2 reduction to formate. Those results showed that π^+-π interactions between the imidazolium cation ($EMIM^+$) in solution and the reduced bipyridine ligand contained within the Rh complex **1** were at the origin of the increased efficiency of the catalyst. In particular, this π^+-π interaction: (*i*) lowered the reduction potential of the complex; (*ii*) increased the free-energy barriers for both CO_2RR and HER pathways, however this effect being much more pronounced for the HER pathway. In the case of the modified electrodes (IM^+_{EE} and IM^+_{EC} cathodes), we hypothesize that the same type of π^+-π interactions occur between the immobilized imidazolium on the electrode and the Rh complex **1**, providing a driving force for concentrating the soluble complex close to the electrode and increasing the selectivity for formate production by inhibiting HER. All these data confirm a common trend in improving CO_2RR catalytic performance (onset potential, current density and FE_{HCOO^-}) using [EMIM][PF_6] either in solution or, even more efficiently, after its grafting on the electrode surface. Not unexpectedly, very minor differences are reported here between IM^+_{EE} and IM^+_{EC} catalytic performances. It is possible that IM^+_{EE} and IM^+_{EC} cathodes with grafted imidazolium (**Figure S3**), provide a higher density of imidazolium at the electrode/electrolyte interface as

compared to that obtained in the case of the bare GC cathode in the presence of $[EMIM]^+$ in solution, explaining the differences in their catalytic performance.

On such a promising ground, we have developed a scaled-up flow cell reactor using such a modified cathode (IM^+_{EE}) and the molecular catalyst solubilized in an acidic aqueous catholyte. The combination of feeding CO_2 as a gas to a carbon-based GDE (allowing to reach industrially relevant current densities such as 100 mA cm^{-2}) with using an acidic electrolyte (to limit CO_2 capture via bicarbonate/carbonate formation in the bulk solution) within a flow cell reactor has no precedent, as far as molecular catalysis is concerned. This new CO_2 conversion system proved stable during consecutive electrolysis provides high and constant production rate of formic acid at industrially relevant current densities (**Figure 5**). Moreover, IM^+_{EE}/GDE cathode divides by two the energy consumption of the process and doubles the $EE_{full\ cell}$ in comparison with bare carbon GDE cathode (**Figure 5b**). So far, the only case of a homogeneous molecular catalyst for CO_2RR tested in a flow cell type reactor is $[Ni(cyclam)]^{2+}$ (cyclam=1,4,8,11-tetraazacyclotetradecane) in CO_2-saturated organic solvents using ferrocene as a sacrificial electron donor[51], but this system is limited by CO_2 solubility in acetonitrile and only current densities lower than 38 mA cm^{-2} were reached. In contrast, the majority of molecular catalysts tested in the literature for CO_2RR in aqueous solution and in a flow cell type reactor have been immobilized on the electrode surface (heterogenized catalysts)[52,53] and in most cases they catalyze CO_2 conversion to CO. In particular, different cobalt phthalocyanine (CoPc)[54,55] and $[Ni(cyclam)]^{2+}$ complexes[56] immobilized on carbon based GDEs implemented in zero-gap membrane reactors has reached high CO production rates. But there are not immobilized complexes for CO_2 conversion to formate reported so far in the literature. Thus, only heterogeneous metal cathodes such as the massive Sn plate cathode[57] and GDEs modified by depositing Sn[58] or SnO_x[59] nanoparticles (operating under alkaline conditions) can be compared to the system reported here in terms of formate production rates (r_{HCOO^-}), and in some cases, of full cell energy efficiency ($EE_{full\ cell}$) and energy consumption (**Table S2**). Interestingly, the r_{HCOO^-} achieved by the combination of 1 mM Rh complex catalyst and the IM^+_{EE}/GDE cathode is 50% higher (from 0.83 to 1.3 g_{HCOO^-} m^{-2} min^{-1}) than the one reached by a Sn plate cathode and half of that obtained by Sn or SnO_x nanoparticles-based GDEs (**Table S2**) under equivalent experimental conditions (but not solution pH), which demonstrates that a homogeneous molecular catalyst properly combined with a smart electrode surface can reach a comparable catalytic performance in terms of production and stability to the one displayed by bi-and tri-dimensional heterogeneous catalysts for CO_2RR.

CONCLUSIONS

Our results demonstrate that the electrocatalytic activity of homogeneous molecular complexes, such as complex **1**, for CO_2RR can be tuned and improved by modifying the surface of carbon electrodes. Specifically, we show that immobilization of imidazolium, a positively charged species, on carbon electrodes promote CO_2 conversion to formate in a broad range of solvents, including acidic aqueous solution, a condition of key importance in order to improve the carbon balance and avoid electrolyte carbonation during CO_2RR. Such an effect of grafted imidazolium can be accounted for its ability to interact with the catalyst favoring CO_2 conversion to formate and for its electrostatic suppressing effect of HER. Thus, the HER suppressing effect displayed by immobilized imidazolium cations represents a cornerstone for the future development of acidic CO_2RR. Notably, this work opens a barely explored pathway to use LEFs induced in CO_2RR by charging the electrode surface with an ionic organic layer (electrolyte immobilization), not only for enhancing environmental relevant electrocatalytic reactions, such as the one described here, but in a broader range of electrochemical applications such as batteries or supercapacitors, where the electrical field and HER suppression need to be finely tuned. This new strategy based on smart electrode surfaces will be potentially useful for impacting activity and selectivity of different electrochemical reactions involving polarizable reactants, intermediates and/or products, which will be sensitive to the strength of the electric field generated at the electrode/electrolyte interface.

ACKNOWLEDGEMENTS

This work was supported by the ‘‘Génie des Procédés’’ PhD Program of Sorbonne Université. E.V. would like to thank the Onassis foundation for financial support (Grant number: F ZO 012-1/ 2018-2019). Y. Adjez thanks Sorbonne Université for the PhD contract. The authors acknowledge the support of the Centre National de la Recherche Scientifique (CNRS) and F. Pillier (Laboratoire Interfaces et Systèmes Electrochimiques, UMR 8235) for the SEM images and EDX analysis.

AUTHOR INFORMATION

Corresponding authors e-mail addresses:

* maria.gomez@college-de-france.fr

* marc.fontecave@college-de-france.fr

* carlos.sanchez@sorbonne-universite.fr

ORCID :

Maria Gomez-Mingot: 0000-0002-1557-2648

Yun Xu-Li: 0000-0003-4805-7156

Marc Fontecave: 0000-0002-8016-4747

Carlos M. Sánchez-Sánchez: 0000-0003-4285-4648

ASSOCIATED CONTENT

Experimental, optimization and additional characterization details and activity evaluation of the different modified electrodes. The Supporting Information is available free of charge at https://pubs.acs.org/doi/xxxxx.

REFERENCES

(1) Shaik, S.; Danovich, D.; Joy, J.; Wang, Z.; Stuyver, T. Electric-Field Mediated Chemistry: Uncovering and Exploiting the Potential of (Oriented) Electric Fields to Exert Chemical Catalysis and Reaction Control. *J. Am. Chem. Soc.* **2020**, *142* (29), 12551–12562.

(2) Stuyver, T.; Ramanan, R.; Mallick, D.; Shaik, S. Oriented (Local) Electric Fields Drive the Millionfold Enhancement of the H-Abstraction Catalysis Observed for Synthetic Metalloenzyme Analogues. *Angew. Chem. Int. Ed.* **2020**, *59* (20), 7915–7920.

(3) Che, F.; Gray, J. T.; Ha, S.; Kruse, N.; Scott, S. L.; McEwen, J.-S. Elucidating the Roles of Electric Fields in Catalysis: A Perspective. *ACS Catal.* **2018**, *8* (6), 5153–5174.

(4) Markovic, N. M. Interfacing Electrochemistry. *Nat. Mater.* **2013**, *12* (2), 101–102.

(5) Amatore, C.; Jutand, A. Anionic Pd(0) and Pd(II) Intermediates in Palladium-Catalyzed Heck and Cross-Coupling Reactions. *Acc. Chem. Res.* **2000**, *33* (5), 314–321.

(6) Nitopi, S.; Bertheussen, E.; Scott, S. B.; Liu, X.; Engstfeld, A. K.; Horch, S.; Seger, B.; Stephens, I. E. L.; Chan, K.; Hahn, C.; Nørskov, J. K.; Jaramillo, T. F.; Chorkendorff, I. Progress and Perspectives of Electrochemical CO2 Reduction on Copper in Aqueous Electrolyte. *Chem. Rev.* **2019**, *119* (12), 7610–7672.

(7) Waegele, M. M.; Gunathunge, C. M.; Li, J.; Li, X. How Cations Affect the Electric Double Layer and the Rates and Selectivity of Electrocatalytic Processes. *J. Chem. Phys.* **2019**, *151* (16), 160902.

(8) Singh, M. R.; Kwon, Y.; Lum, Y.; Ager, J. W. I.; Bell, A. T. Hydrolysis of Electrolyte Cations Enhances the Electrochemical Reduction of CO2 over Ag and Cu. *J. Am. Chem. Soc.* **2016**, *138* (39), 13006–13012.

(9) Ayemoba, O.; Cuesta, A. Spectroscopic Evidence of Size-Dependent Buffering of Interfacial pH by Cation Hydrolysis during CO2 Electroreduction. *ACS Appl. Mater. Interfaces* **2017**, *9* (33), 27377–27382.

(10) Hussain, G.; Pérez-Martínez, L.; Le, J.-B.; Papasizza, M.; Cabello, G.; Cheng, J.; Cuesta, A. How Cations Determine the Interfacial Potential Profile: Relevance for the CO2 Reduction Reaction. *Electrochimica Acta* **2019**, *327*, 135055.

(11) Yang, X.-H.; Papasizza, M.; Cuesta, A.; Cheng, J. Water-In-Salt Environment Reduces the Overpotential for Reduction of CO2 to CO2– in Ionic Liquid/Water Mixtures. *ACS Catal.* **2022**, *12* (11), 6770–6780.

(12) Resasco, J.; Chen, L. D.; Clark, E.; Tsai, C.; Hahn, C.; Jaramillo, T. F.; Chan, K.; Bell, A. T. Promoter Effects of Alkali Metal Cations on the Electrochemical Reduction of Carbon Dioxide. *J. Am. Chem. Soc.* **2017**, *139* (32), 11277–11287.

(13) Monteiro, M. C. O.; Dattila, F.; Hagedoorn, B.; García-Muelas, R.; López, N.; Koper, M. T. M. Absence of CO2 Electroreduction on Copper, Gold and Silver Electrodes without Metal Cations in Solution. *Nat. Catal.* **2021**, *4* (8), 654–662.

(14) Huang, J. E.; Li, F.; Ozden, A.; Sedighian Rasouli, A.; García de Arquer, F. P.; Liu, S.; Zhang, S.; Luo, M.; Wang, X.; Lum, Y.; Xu, Y.; Bertens, K.; Miao, R. K.; Dinh, C.-T.; Sinton, D.; Sargent, E. H. CO2 Electrolysis to Multicarbon Products in Strong Acid. *Science* **2021**, *372* (6546), 1074–1078.

(15) Merino-Garcia, I.; Tinat, L.; Albo, J.; Alvarez-Guerra, M.; Irabien, A.; Durupthy, O.; Vivier, V.; Sánchez-Sánchez, C. M. Continuous Electroconversion of CO2 into Formate Using 2 Nm Tin Oxide Nanoparticles. *Appl. Catal. B Environ.* **2021**, *297*, 120447–120458.

(16) Thijs, B.; Rongé, J.; Martens, J. A. Matching Emerging Formic Acid Synthesis Processes with Application Requirements. *Green Chem.* **2022**, *24* (6), 2287–2295.

(17) Monteiro, M. C. O.; Dattila, F.; López, N.; Koper, M. T. M. The Role of Cation Acidity on the Competition between Hydrogen Evolution and CO2 Reduction on Gold Electrodes. *J. Am. Chem. Soc.* **2022**, *144* (4), 1589–1602.
(18) Vichou, E.; Solé-Daura, A.; Mellot-Draznieks, C.; Li, Y.; Gomez-Mingot, M.; Fontecave, M.; Sánchez-Sánchez, C. M. Electrocatalytic Conversion of CO2 to Formate at Low Overpotential by Electrolyte Engineering in Model Molecular Catalysis. *ChemSusChem* **2022**, *15* (24), e202201566.
(19) Lau, G. P. S.; Schreier, M.; Vasilyev, D.; Scopelliti, R.; Grätzel, M.; Dyson, P. J. New Insights Into the Role of Imidazolium-Based Promoters for the Electroreduction of CO2 on a Silver Electrode. *J. Am. Chem. Soc.* **2016**, *138* (25), 7820–7823.
(20) Thevenon, A.; Rosas-Hernández, A.; Fontani Herreros, A. M.; Agapie, T.; Peters, J. C. Dramatic HER Suppression on Ag Electrodes via Molecular Films for Highly Selective CO2 to CO Reduction. *ACS Catal.* **2021**, *11* (8), 4530–4537.
(21) Koshy, D. M.; Akhade, S. A.; Shugar, A.; Abiose, K.; Shi, J.; Liang, S.; Oakdale, J. S.; Weitzner, S. E.; Varley, J. B.; Duoss, E. B.; Baker, S. E.; Hahn, C.; Bao, Z.; Jaramillo, T. F. Chemical Modifications of Ag Catalyst Surfaces with Imidazolium Ionomers Modulate H2 Evolution Rates during Electrochemical CO2 Reduction. *J. Am. Chem. Soc.* **2021**, *143* (36), 14712–14725.
(22) Sha, Y.; Zhang, J.; Cheng, X.; Xu, M.; Su, Z.; Wang, Y.; Hu, J.; Han, B.; Zheng, L. Anchoring Ionic Liquid in Copper Electrocatalyst for Improving CO2 Conversion to Ethylene. *Angew. Chem. Int. Ed.* **2022**, *61* (13), e202200039.
(23) Nie, W.; Heim, G. P.; Watkins, N. B.; Agapie, T.; Peters, J. C. Organic Additive-derived Films on Cu Electrodes Promote Electrochemical CO $_2$ Reduction to C $_{2+}$ Products Under Strongly Acidic Conditions. *Angew. Chem. Int. Ed.* **2023**, *62* (12), e202216102.
(24) Wakerley, D.; Lamaison, S.; Ozanam, F.; Menguy, N.; Mercier, D.; Marcus, P.; Fontecave, M.; Mougel, V. Bio-Inspired Hydrophobicity Promotes CO2 Reduction on a Cu Surface. *Nat. Mater.* **2019**, *18* (11), 1222–1227.
(25) Liang, H.-Q.; Zhao, S.; Hu, X.-M.; Ceccato, M.; Skrydstrup, T.; Daasbjerg, K. Hydrophobic Copper Interfaces Boost Electroreduction of Carbon Dioxide to Ethylene in Water. *ACS Catal.* **2021**, *11* (2), 958–966.
(26) Creissen, C. E.; Rivera de la Cruz, J. G.; Karapinar, D.; Taverna, D.; Schreiber, M. W.; Fontecave, M. Molecular Inhibition for Selective CO2 Conversion. *Angew. Chem. Int. Ed.* **2022**, *61* (32), e202206279.
(27) Li, F.; Thevenon, A.; Rosas-Hernández, A.; Wang, Z.; Li, Y.; Gabardo, C. M.; Ozden, A.; Dinh, C. T.; Li, J.; Wang, Y.; Edwards, J. P.; Xu, Y.; McCallum, C.; Tao, L.; Liang, Z.-Q.; Luo, M.; Wang, X.; Li, H.; O'Brien, C. P.; Tan, C.-S.; Nam, D.-H.; Quintero-Bermudez, R.; Zhuang, T.-T.; Li, Y. C.; Han, Z.; Britt, R. D.; Sinton, D.; Agapie, T.; Peters, J. C.; Sargent, E. H. Molecular Tuning of CO2-to-Ethylene Conversion. *Nature* **2020**, *577* (7791), 509–513.
(28) Chen, X.; Chen, J.; Alghoraibi, N. M.; Henckel, D. A.; Zhang, R.; Nwabara, U. O.; Madsen, K. E.; Kenis, P. J. A.; Zimmerman, S. C.; Gewirth, A. A. Electrochemical CO2-to-Ethylene Conversion on Polyamine-Incorporated Cu Electrodes. *Nat. Catal.* **2021**, *4* (1), 20–27.
(29) Kutz, R. B.; Chen, Q.; Yang, H.; Sajjad, S. D.; Liu, Z.; Masel, I. R. Sustainion Imidazolium-Functionalized Polymers for Carbon Dioxide Electrolysis. *Energy Technol.* **2017**, *5* (6), 929–936.
(30) Kaczur, J. J.; Yang, H.; Liu, Z.; Sajjad, S. D.; Masel, R. I. A Review of the Use of Immobilized Ionic Liquids in the Electrochemical Conversion of CO2. *C* **2020**, *6* (2), 33. c6020033. 12

(31) Wang, W.-H.; Suna, Y.; Himeda, Y.; Muckerman, J. T.; Fujita, E. Functionalized Cyclopentadienyl Rhodium(III) Bipyridine Complexes: Synthesis, Characterization, and Catalytic Application in Hydrogenation of Ketones. *Dalton Trans.* **2013**, *42* (26), 9628–9636.
(32) Kölle, U.; Grützel, M. Organometallic Rhodium(III) Complexes as Catalysts for the Photoreduction of Protons to Hydrogen on Colloidal TiO2. *Angew. Chem. Int. Ed. Engl.* **1987**, *26* (6), 567–570.
(33) Bouden, S.; Gómez-Mingot, M.; Randriamahazaka, H.; Ghilane, J. Surface Initiated Immobilization of Molecules Contained in an Ionic Liquid Framework. *Anal. Chem.* **2016**, *88* (1), 1017–1021.
(34) Wang, Y.; Hayashi, T.; He, D.; Li, Y.; Jin, F.; Nakamura, R. A Reduced Imidazolium Cation Layer Serves as the Active Site for Electrochemical Carbon Dioxide Reduction. *Appl. Catal. B Environ.* **2020**, *264*, 118495–118502.
(35) Katsyuba, S. A.; Dyson, P. J.; Vandyukova, E. E.; Chernova, A. V.; Vidiš, A. Molecular Structure, Vibrational Spectra, and Hydrogen Bonding of the Ionic Liquid 1-Ethyl-3-Methyl-1H-Imidazolium Tetrafluoroborate. *Helv. Chim. Acta* **2004**, *87* (10), 2556–2565.
(36) Papasizza, M.; Cuesta, A. In Situ Monitoring Using ATR-SEIRAS of the Electrocatalytic Reduction of CO_2 on Au in an Ionic Liquid/Water Mixture. *ACS Catal.* **2018**, *8* (7), 6345–6352.
(37) Cuesta, A. ATR-SEIRAS for Time-Resolved Studies of Electrode–Electrolyte Interfaces. *Curr. Opin. Electrochem.* **2022**, *35*, 101041.
(38) Chi, Y. S.; Hwang, S.; Lee, B. S.; Kwak, J.; Choi, I. S.; Lee, S. Anion Exchange-Promoted Ru3+/2+ Redox Switch in Self-Assembled Monolayers of Imidazolium Ions on a Gold Electrode. *Langmuir* **2005**, *21* (10), 4268–4271.
(39) Candia-Onfray, C.; Bollo, S.; Yáñez, C.; Escalona, N.; Marco, J. F.; Menéndez, N.; Salazar, R.; Recio, F. J. Nanostructured Fe-N-C Pyrolyzed Catalyst for the H2O2 Electrochemical Sensing. *Electrochimica Acta* **2021**, *387*, 138468.
(40) Men, S.; Mitchell, D. S.; Lovelock, K. R. J.; Licence, P. X-Ray Photoelectron Spectroscopy of Pyridinium-Based Ionic Liquids: Comparison to Imidazolium- and Pyrrolidinium-Based Analogues. *ChemPhysChem* **2015**, *16* (10), 2211–2218.
(41) Villar-Garcia, I. J.; Smith, E. F.; Taylor, A. W.; Qiu, F.; Lovelock, K. R. J.; Jones, R. G.; Licence, P. Charging of Ionic Liquid Surfaces under X-Ray Irradiation: The Measurement of Absolute Binding Energies by XPS. *Phys Chem Chem Phys* **2011**, *13* (7), 2797–2808.
(42) Michez, R.; Vander Steen, J.; Doneux, T.; Luhmer, M.; Buess-Herman, C. Electroreduction of 1-Butyl-3-Methylimidazolium Bis(Trifluoromethanesulfonyl)Imide Ionic Liquid: Oriented Product Selectivity through the Electrode Material. *Electrochimica Acta* **2018**, *270*, 434–439.
(43) Michez, R.; Doneux, T.; Buess-Herman, C.; Luhmer, M. NMR Study of the Reductive Decomposition of [BMIm][NTf2] at Gold Electrodes and Indirect Electrochemical Conversion of CO2. *ChemPhysChem* **2017**, *18* (16), 2208–2216.
(44) Feroci, M.; Chiarotto, I.; Forte, G.; Inesi, A. An Electrochemical Methodology for the Cyclic CO2 "Catch and Release". The Role of the Electrogenerated N-Heterocyclic Carbene in BMIm-BF4. *J. CO2 Util.* **2013**, *2* (Complete), 29–34.
(45) Hanc-Scherer, F. A.; Montiel, M. A.; Montiel, V.; Herrero, E.; Sánchez-Sánchez, C. M. Surface Structured Platinum Electrodes for the Electrochemical Reduction of Carbon Dioxide in Imidazolium Based Ionic Liquids. *Phys. Chem. Chem. Phys.* **2015**, *17* (37), 23909–23916.
(46) Bard A. J. and Faulkner L. R. *Electrochemical Methods: Fundamentals and Applications*, John Wiley and Sons.; New York, NY, 2001.

(47) Bard, A. J. Inner-Sphere Heterogeneous Electrode Reactions. Electrocatalysis and Photocatalysis: The Challenge. *J. Am. Chem. Soc.* **2010**, *132* (22), 7559–7567.
(48) Feaster, J. T.; Jongerius, A. L.; Liu, X.; Urushihara, M.; Nitopi, S. A.; Hahn, C.; Chan, K.; Nørskov, J. K.; Jaramillo, T. F. Understanding the Influence of [EMIM]Cl on the Suppression of the Hydrogen Evolution Reaction on Transition Metal Electrodes. *Langmuir* **2017**, *33* (37), 9464–9471.
(49) Higgins, D.; Hahn, C.; Xiang, C.; Jaramillo, T. F.; Weber, A. Z. Gas-Diffusion Electrodes for Carbon Dioxide Reduction: A New Paradigm. *ACS Energy Lett.* **2019**, *4* (1), 317–324.
(50) De Mot, B.; Hereijgers, J.; Duarte, M.; Breugelmans, T. Influence of Flow and Pressure Distribution inside a Gas Diffusion Electrode on the Performance of a Flow-by CO2 Electrolyzer. *Chem. Eng. J.* **2019**, *378*, 122224.
(51) Jiang, C.; Nichols, A. W.; Walzer, J. F.; Machan, C. W. Electrochemical CO2 Reduction in a Continuous Non-Aqueous Flow Cell with [Ni(Cyclam)]2+. *Inorg. Chem.* **2020**, *59* (3), 1883–1892.
(52) Torbensen, K.; Boudy, B.; Joulié, D.; von Wolff, N.; Robert, M. Emergence of CO2 Electrolyzers Including Supported Molecular Catalysts. *Curr. Opin. Electrochem.* **2020**, *24*, 49–55.
(53) Lei, K.; Yu Xia, B. Electrocatalytic CO2 Reduction: From Discrete Molecular Catalysts to Their Integrated Catalytic Materials. *Chem. – Eur. J.* **2022**, *28* (30), e202200141.
(54) Ren, S.; Joulié, D.; Salvatore, D.; Torbensen, K.; Wang, M.; Robert, M.; Berlinguette, C. P. Molecular Electrocatalysts Can Mediate Fast, Selective CO_2 Reduction in a Flow Cell. *Science* **2019**, *365* (6451), 367-369.
(55) Wang, M.; Torbensen, K.; Salvatore, D.; Ren, S.; Joulié, D.; Dumoulin, F.; Mendoza, D.; Lassalle-Kaiser, B.; Işci, U.; Berlinguette, C. P.; Robert, M. CO2 Electrochemical Catalytic Reduction with a Highly Active Cobalt Phthalocyanine. *Nat. Commun.* **2019**, *10* (1), 3602.
(56) Siritanaratkul, B.; Forster, M.; Greenwell, F.; Sharma, P. K.; Yu, E. H.; Cowan, A. J. Zero-Gap Bipolar Membrane Electrolyzer for Carbon Dioxide Reduction Using Acid-Tolerant Molecular Electrocatalysts. *J. Am. Chem. Soc.* **2022**, *144* (17), 7551–7556.
(57) Alvarez-Guerra, M.; Del Castillo, A.; Irabien, A. Continuous Electrochemical Reduction of Carbon Dioxide into Formate Using a Tin Cathode: Comparison with Lead Cathode. *Chem. Eng. Res. Des.* **2014**, *92* (4), 692–701.
(58) Del Castillo, A.; Alvarez-Guerra, M.; Solla-Gullón, J.; Sáez, A.; Montiel, V.; Irabien, A. Sn Nanoparticles on Gas Diffusion Electrodes: Synthesis, Characterization and Use for Continuous CO 2 Electroreduction to Formate. *J. CO2 Util.* **2017**, *18*, 222–228.
(59) Li, M.; Idros, M. N.; Wu, Y.; Garg, S.; Gao, S.; Lin, R.; Rabiee, H.; Li, Z.; Ge, L.; Rufford, T. E.; Zhu, Z.; Li, L.; Wang, G. Unveiling the Effects of Dimensionality of Tin Oxide-Derived Catalysts on CO2 Reduction by Using Gas-Diffusion Electrodes. *React. Chem. Eng.* **2021**, *6* (2), 345–352.

SUPPORTING INFORMATION

Smart electrode surfaces by electrolyte immobilization for electrocatalytic CO_2 conversion

Elli Vichou[†,‡], Yanis Adjez[‡], Yun Li[†], Maria Gomez-Mingot[†,], Marc Fontecave[†,*] and Carlos M. Sánchez-Sánchez[‡,*]*

[†]Laboratoire de Chimie des Processus Biologiques, Collège de France, UMR 8229 CNRS, Sorbonne Université, PSL Research University, 11 Place Marcelin Berthelot, 75005 Paris, France

[‡]Sorbonne Université, CNRS, Laboratoire Interfaces et Systèmes Electrochimiques, LISE, 4 Place Jussieu, 75005 Paris, France

AUTHOR INFORMATION

Corresponding authors e-mail addresses:

* maria.gomez@college-de-france.fr

* marc.fontecave@college-de-france.fr

* carlos.sanchez@sorbonne-universite.fr

Table of Contents

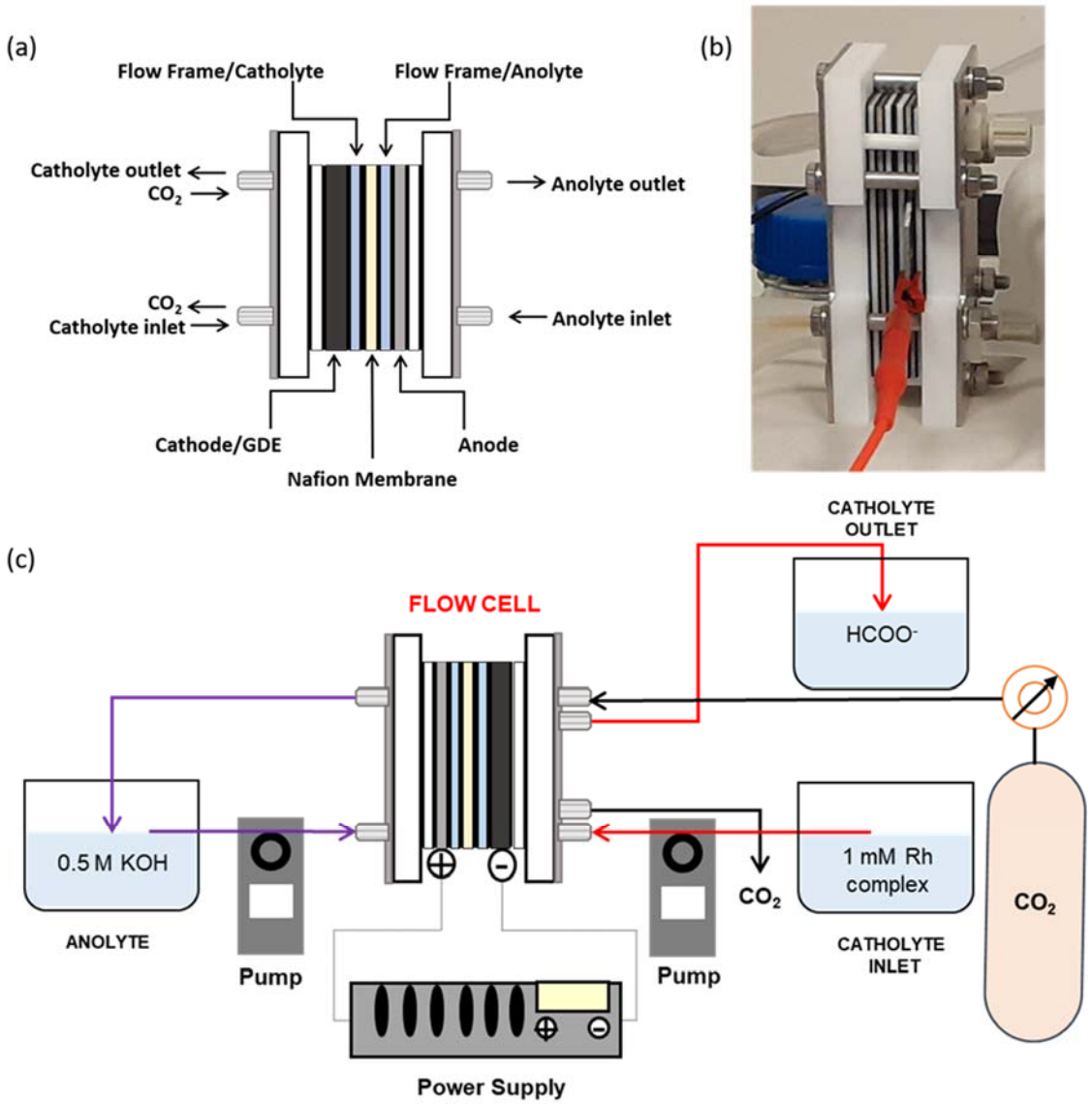

Figure S1. (a) Flow cell type reactor used for scaling up CO_2RR. (b) Picture of the full flow cell type reactor assembly (c) Schematic representation of the scaled experimental setup for CO_2 gas conversion in a flow cell reactor.

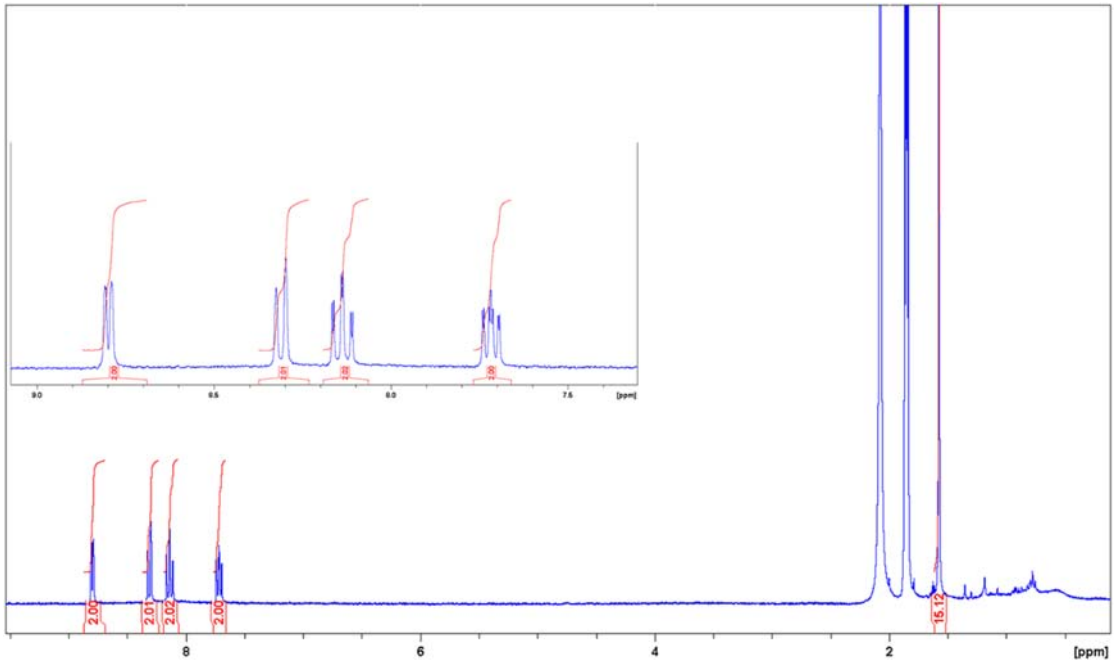

Figure S2. ^{1}H NMR (300 MHz, CD_3CN) of synthesized [Rh(bpy)(Cp*)Cl]: δ/ppm, 1.61 (s, 15H), 7.71 (ψt, J = 7.2 Hz, 2H), 8.13 (dt, J = 7.7 Hz, 2H), 8.30 (d, J = 8.0 Hz, 2H), 8.78 (d, J = 5.5 Hz, 2H).

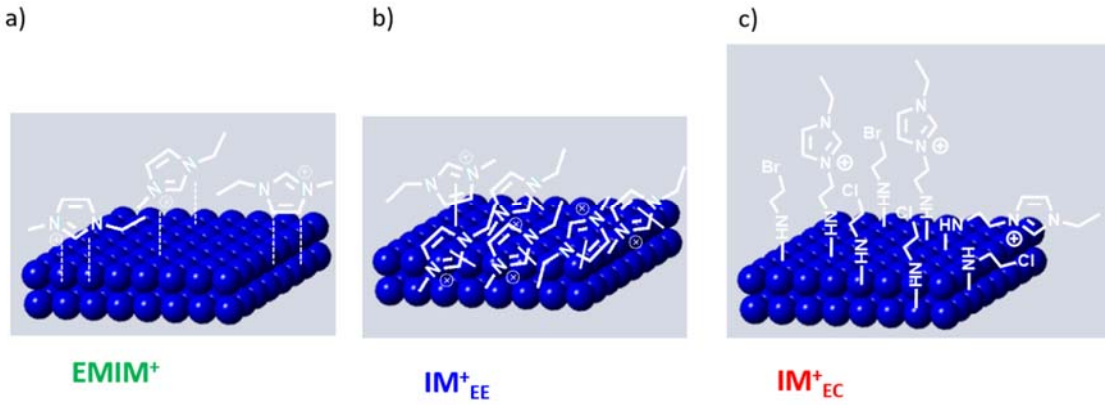

Figure S3. Schematic representation of the electrode surface a) $EMIM^+$ in solution, b) IM^+_{EE} and c) IM^+_{EC}.

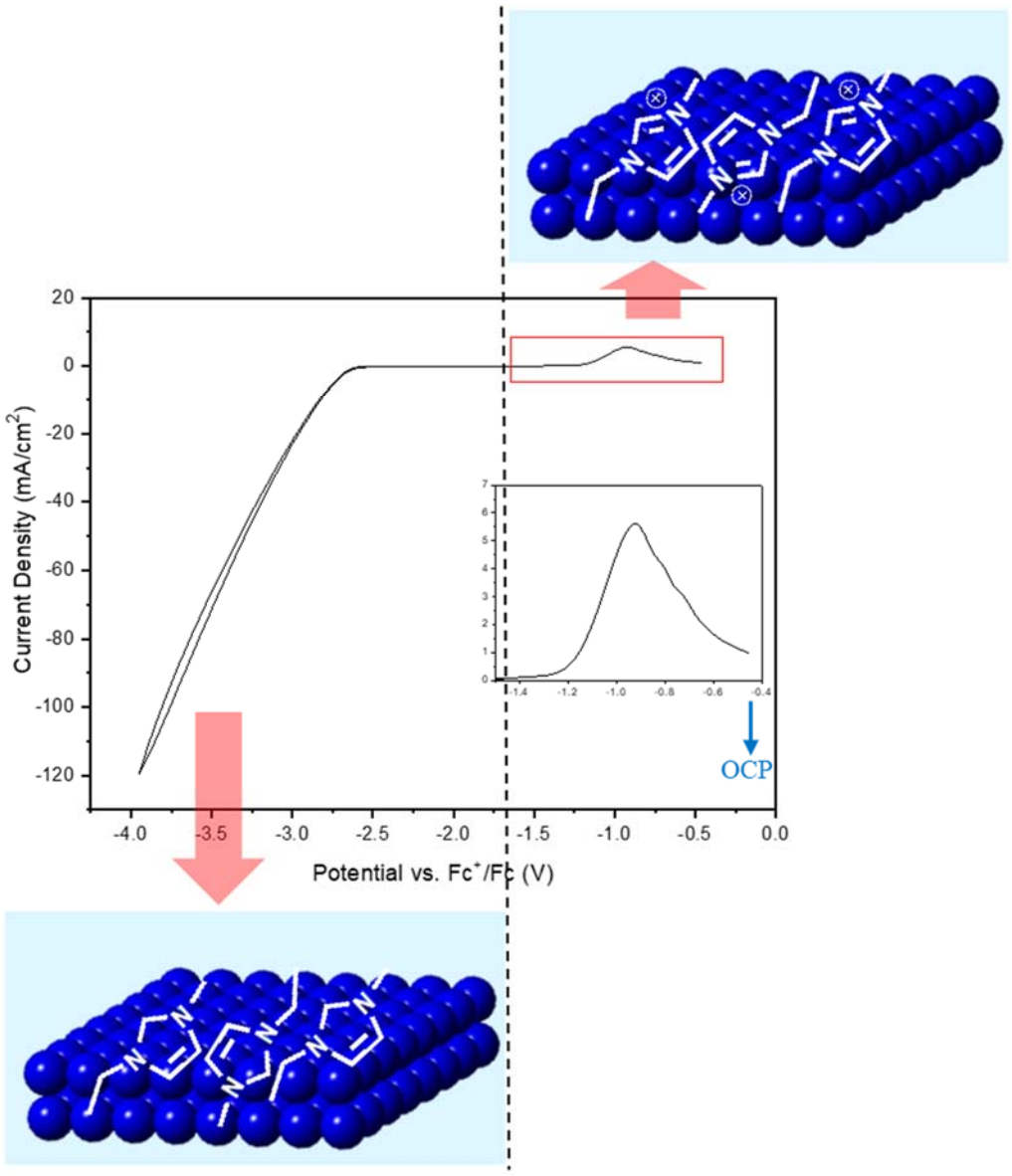

Figure S4. Imidazolium layer formation (IM^{+}_{EE}) on a 3 mm GCE. Firstly, the electroreduction of 0.5 M [EMIM][PF_6] in Ar saturated acetonitrile solution in the forward sweep from -1.45 to -3.95 V *vs.* Fc^{+}/Fc. Secondly, the electrooxidation by scanning the potential positively up to -0.45 V *vs.* Fc^{+}/Fc (OCP) in the reverse scan. Inset shows a zoom on the oxidation peak region. Scan rate 0.1 V s^{-1}.

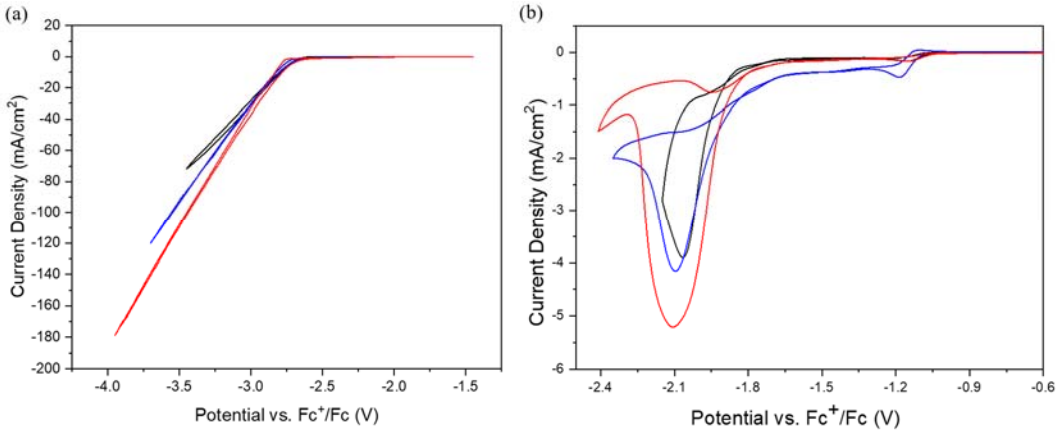

Figure S5. (a) Optimization of IM^{+}_{EE} synthesis in Ar saturated 0.5 M [EMIM][PF_6] acetonitrile solution by CV reaching different potential windows at 0.1 V s^{-1}. (b) Characterization CVs of IM^{+}_{EE} in 1 mM complex 1 and 0.5 M [TBA][PF_6] acetonitrile solution containing 5% v/v H_2O under CO_2 at 0.01 V s^{-1}. Color code: from -1.45 to -3.45 V *vs.* Fc^{+}/Fc (black plot), from -1.45 to -3.75 V *vs.* Fc^{+}/Fc (blue plot), and from -1.45 to -3.95 V *vs.* Fc^{+}/Fc (red plot). Working electrode: 3 mm GCE.

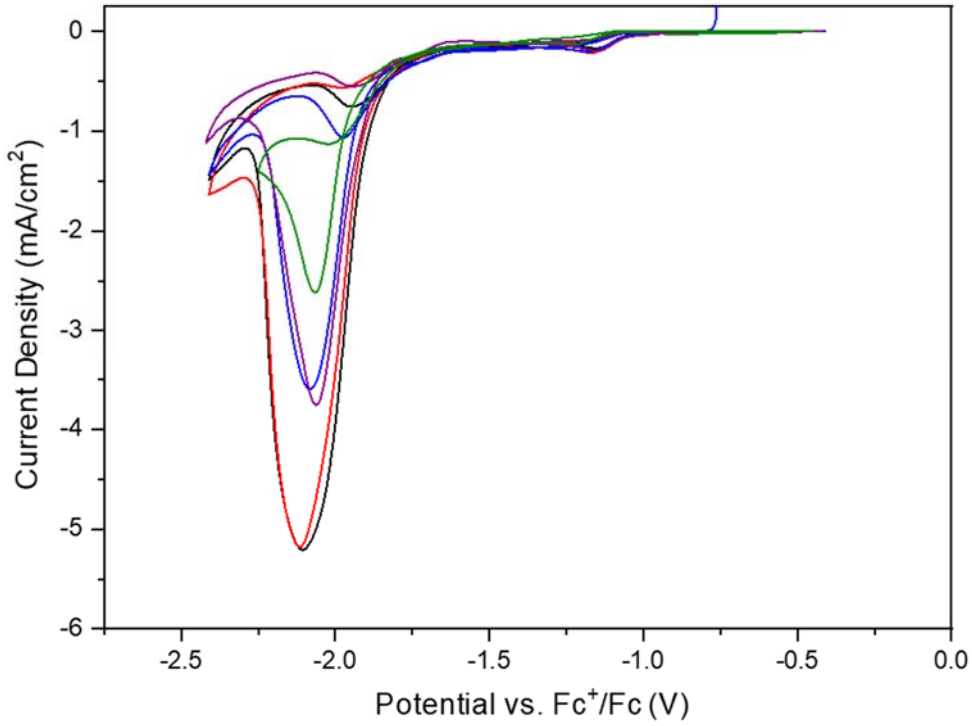

Figure S6. Characterization CVs of IM^{+}_{EE} synthesized in Ar saturated 0.5 M [EMIM][PF_6] acetonitrile solution by CA at -3.95 V *vs.* Fc^+/Fc for different duration. Color code: 10 s (red plot), 30 s (blue plot), 60 s (purple plot), 15 min (green plot). It is also shown for comparison the characterization CV of IM^{+}_{EE} synthesized by 1 CV reaching -3.95 V at 0.1 V s^{-1} (black plot). Working electrode: 3 mm GCE. Solution composition: 1 mM complex 1 and 0.5 M [TBA][PF_6] in acetonitrile solution containing 5% v/v H_2O under CO_2 at 0.01 V s^{-1}.

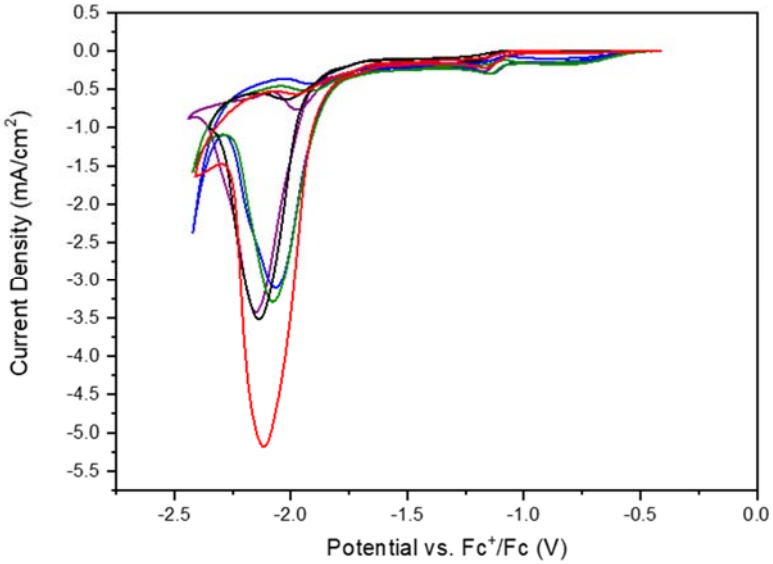

Figure S7. Characterization CVs of IM^+_{EE} synthesized in Ar saturated acetonitrile solution containing different concentrations of [EMIM][PF_6] by CA at -3.95 V *vs.* Fc^+/Fc for 10 s. Color code: 0.01 M (black plot), 0.1 M (blue plot), 0.5 M (red plot) and 1 M [EMIM][PF_6] (green plot). It is also shown for comparison the characterization CV of a bare GCE (purple plot). Working electrode: 3 mm GCE. Solution composition: 1 mM complex 1 and 0.5 M [TBA][PF_6] in acetonitrile solution containing 5% v/v H_2O under CO_2 at 0.01 V s^{-1}.

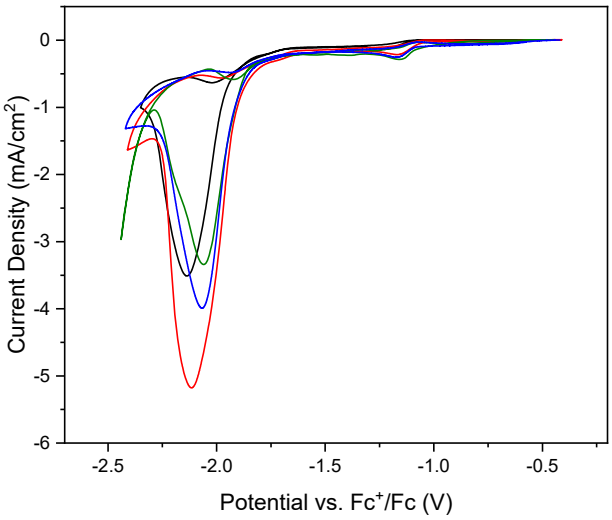

Figure S8. Characterization CVs of IM^{+}_{EE} synthesized in Ar saturated acetonitrile solution containing 0.5 M of different imidazolium-based ILs by CA at -3.95 V *vs.* Fc^+/Fc for 10 s. Color code: 0.5 M [EMIM][PF_6] (red plot), 0.5 M [BMIM][PF_6] (green plot), 0.5 M of [EDMIM][PF_6] (blue plot). It is also shown for comparison the characterization CV of a bare GCE (black plot). Working electrode: 3 mm GCE. Solution composition: 1 mM complex 1 and 0.5 M [TBA][PF_6] in acetonitrile solution containing 5% v/v H_2O under CO_2 at 0.01 V s^{-1}.

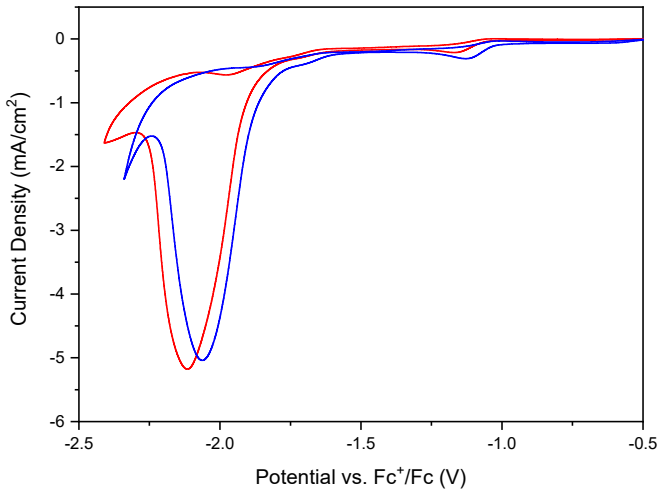

Figure S9. Characterization CVs of IM^+_{EE} synthesized in Ar saturated acetonitrile solution containing 0.5 M of different imidazolium-based ILs by CA at -3.95 V *vs.* Fc^+/Fc for 10 s. Color code: 0.5 M [EMIM][PF_6] (red plot) and 0.5 M of [EMIM][BF_4] (blue plot).Working electrode: 3 mm GCE. Solution composition: 1 mM complex 1 and 0.5 M [TBA][PF_6] in acetonitrile solution containing 5% v/v H_2O under CO_2 at 0.01 V s^{-1}.

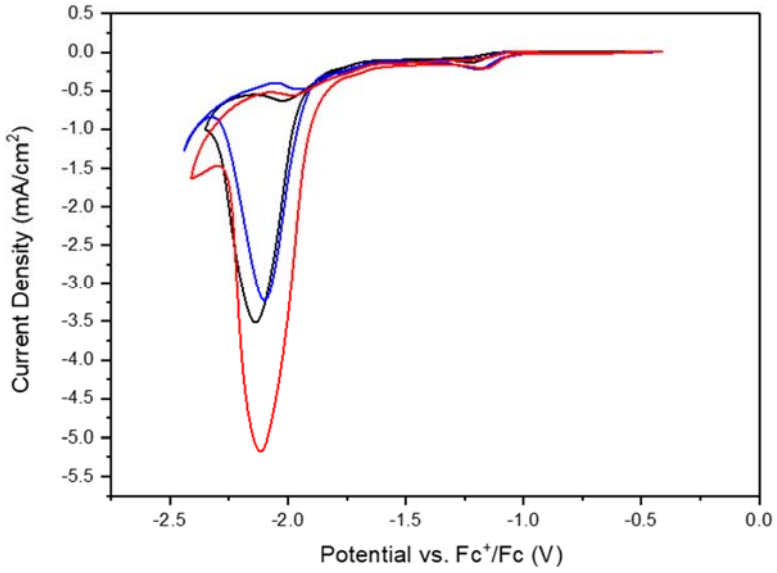

Figure S10. Characterization CVs of IM^{+}_{EE} synthesized in 0.5 M [EMIM][PF_6] acetonitrile solution by CA at -3.95 V *vs.* Fc^{+}/Fc for 10 s. Color code: Ar saturated solution (red plot) and CO_2 saturated solution (blue plot). It is also shown for comparison the characterization CV of a bare GCE (black plot). Working electrode: 3 mm GCE. Solution composition: 1 mM complex 1 and 0.5 M [TBA][PF_6] in acetonitrile solution containing 5% v/v H_2O under CO_2 at 0.01 V s^{-1}.

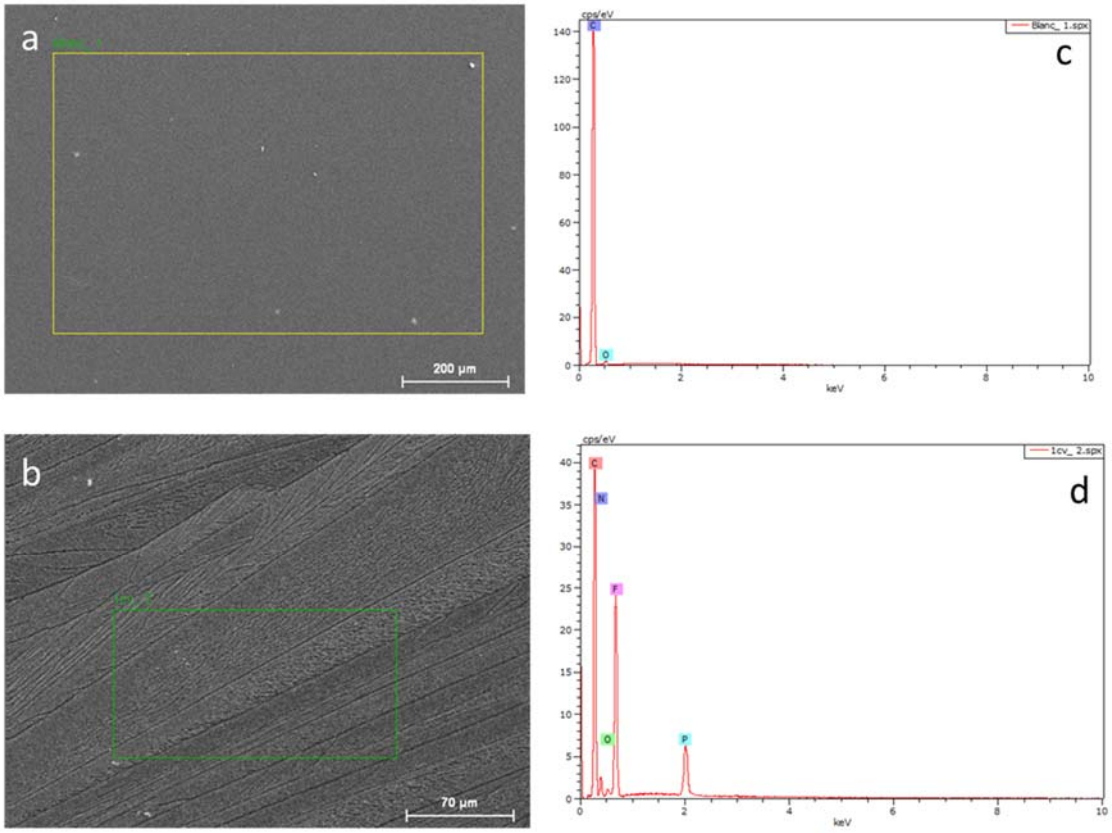

Figure S11. SEM image and Energy Dispersive X-Ray (EDX) analysis of bare GC cathode (a) and (c), respectively. SEM image and EDX analysis of modified IM^{+}_{EE} cathode synthesized in 0.5 M [EMIM][PF_6] acetonitrile solution (b) and (d), respectively.

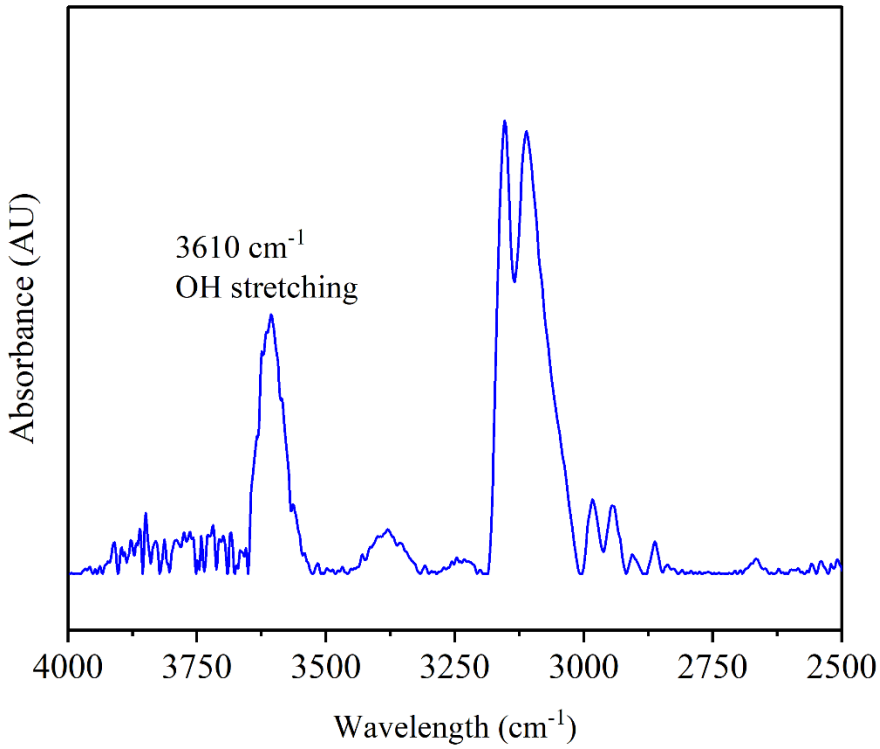

Figure S12. Spectroscopic characterization of IM^{+}_{EE} cathode by ATR-FTIR in the high wavelength region (4000-2500 cm^{-1}).

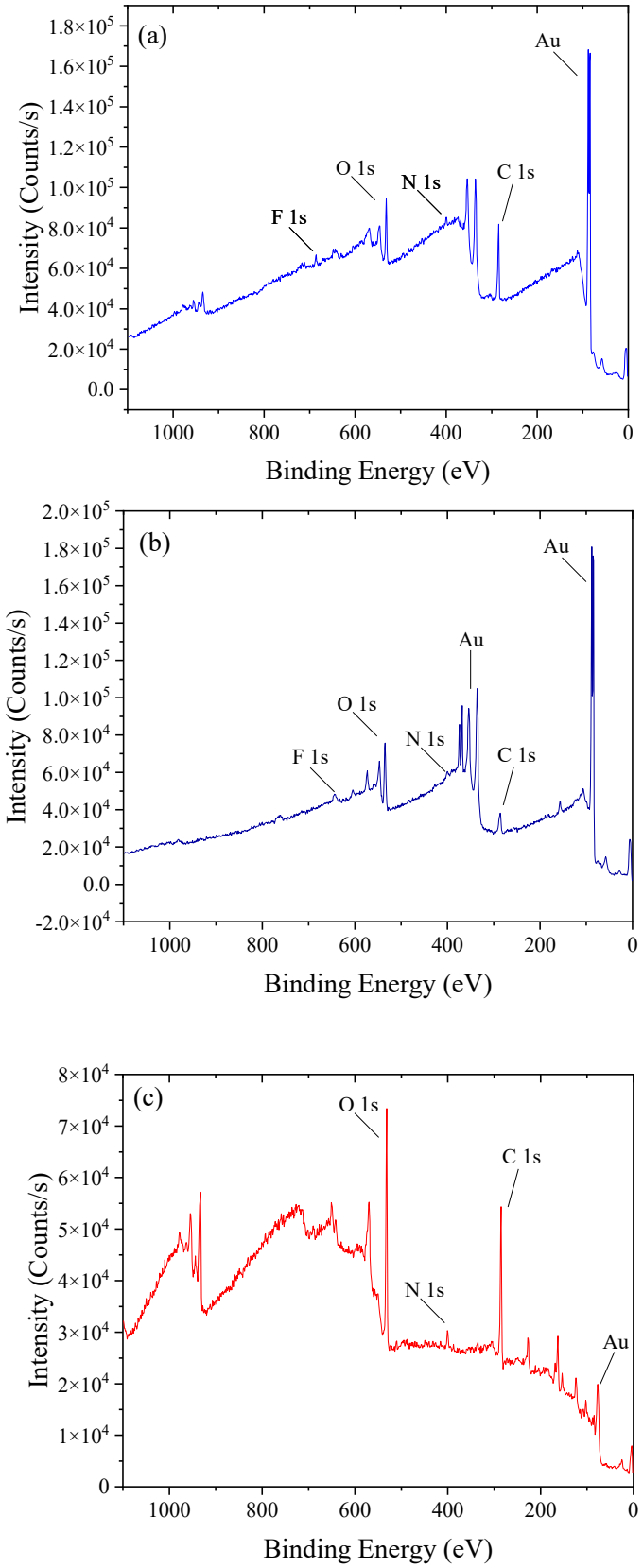

Figure S13. Overall XPS survey spectra for imidazolium supported layers on gold electrode. (a) IM^{+}_{EE} cathode synthesized in Ar saturated 0.5 M [EMIM][PF_6] acetonitrile solution. (b) IM^{+}_{EE} cathode synthesized in Ar saturated 0.5 M [EMIM][BF_4] aqueous solution. (c) IM^{+}_{EC} cathode.

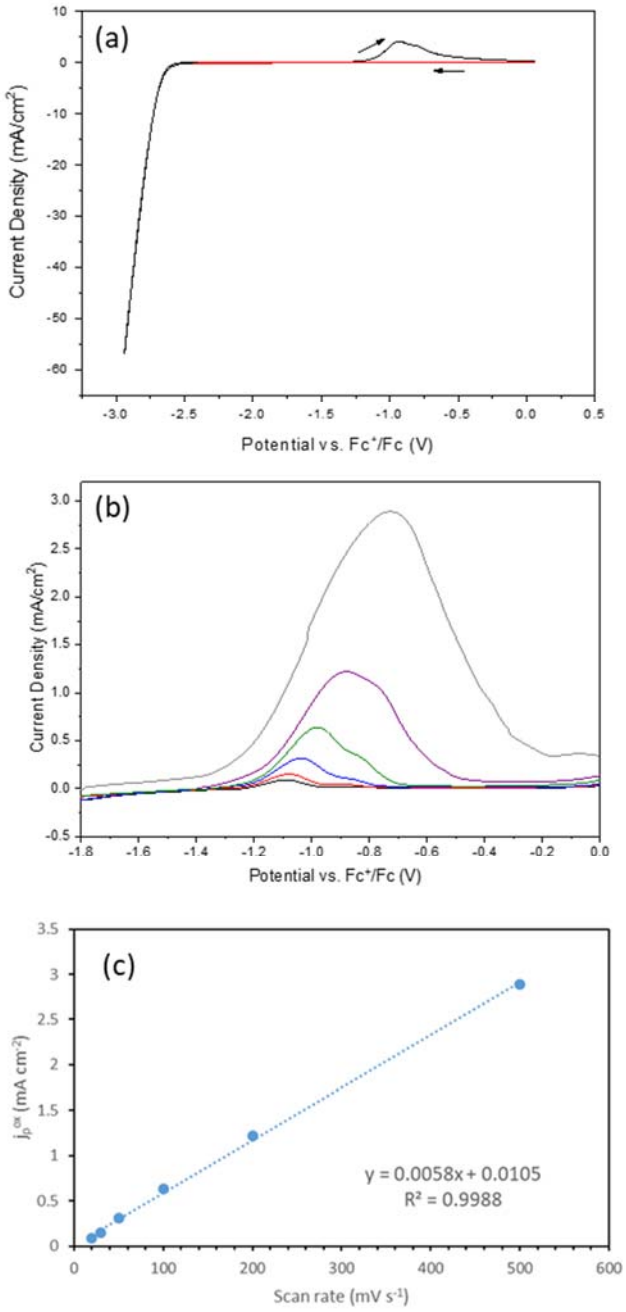

Figure S14. Formation of the imidazolium layer (IM^{+}_{EE}) on a 3 mm GC disc electrode using an Ar saturated acetonitrile solution containing 0.5 M [EMIM][PF_6]. (a) CV cycles scanning down to -2.95 V *vs.* Fc^{+}/Fc (black plot) and to -2.45 V *vs.* Fc^{+}/Fc (red plot) at 0.1 V s^{-1} (small arrows indicate the scan direction). (b) Zoom on the anodic peak obtained by linear sweep voltammetry (LSV) after a reduction step at -2.95 V *vs.* Fc^{+}/Fc for 10 s by chronoamperometry. Different colors represent the variation on the potential scan rate during LSV from 20 to 500 mV s^{-1}. (c) Plot of the maximum oxidation current density at the peak potential (j_p^{ox}) in LSV as a function of potential scan rate.

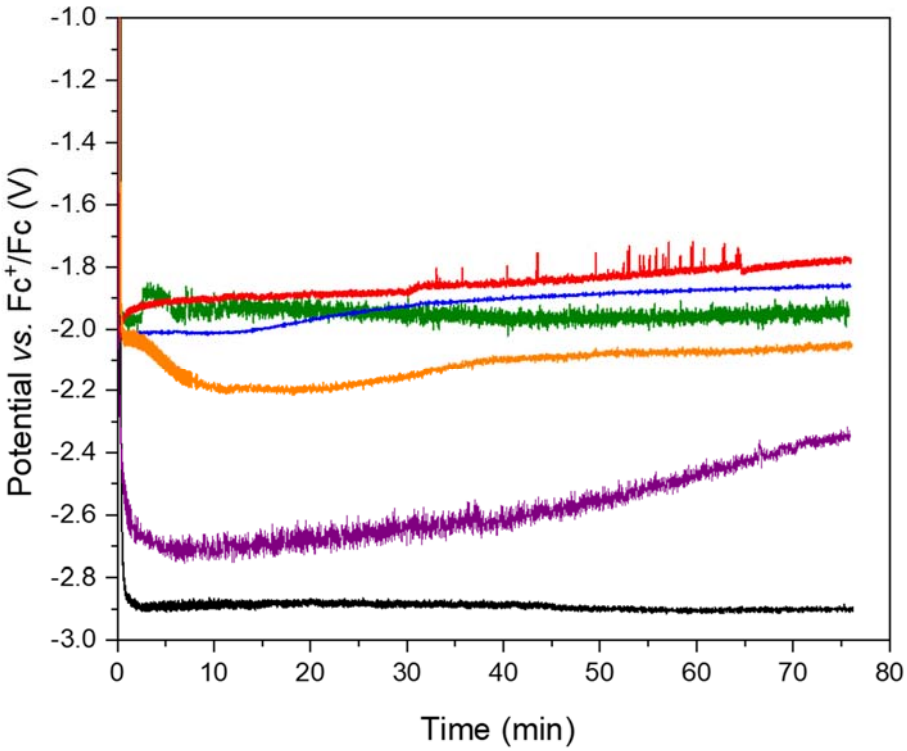

Figure S15. Constant current electrolysis at -3.33 mA cm^{-2} of 1 mM Rh complex in acetonitrile solution under CO_2 in presence of 5 % (vol.) H_2O on: a bare GC cathode in 0.5 M [TBA][PF_6] (black plot), a bare GC cathode in 0.5 M [EMIM][PF_6] (green plot), an IM^{+}_{EE} cathode in 0.5 M [TBA][PF_6] (blue plot) and an IM^{+}_{EC} cathode in 0.5 M [TBA][PF_6] (red plot). Also, CCE at -3.33 mA cm^{-2} of 1 mM Rh complex in acetonitrile: H_2O 50:50 vol. solution under CO_2 on: a bare GC cathode in 0.5 M [TBA][BF_4] (purple plot) and an IM^{+}_{EE} cathode in 0.5 M [TBA][BF_4] (orange plot). Stirring rate: 400 rpm. Electrolysis time: 77 min.

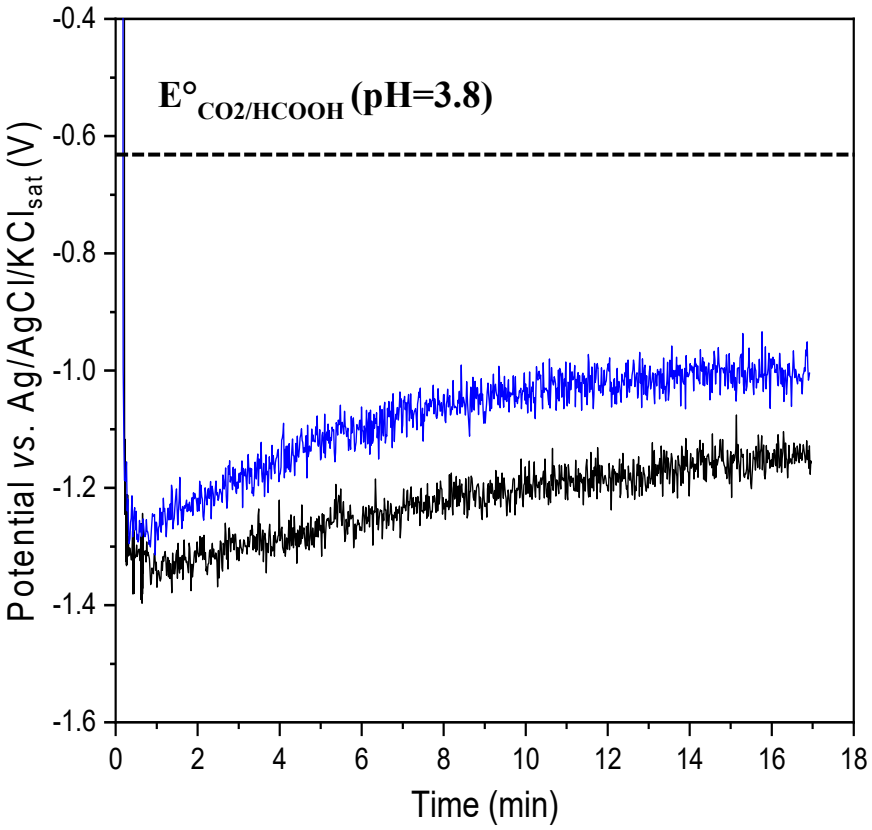

Figure S16. Constant current electrolysis at -3.33 mA cm^{-2} of 1 mM Rh complex in a 0.1 M [TBA][BF_4] and 0.1 M acetate buffer (pH=3.8) aqueous solution under CO_2 on a: bare 3-dimensional reticulated vitreous carbon (RVC, black plot) and IM^{+}_{EE} RVC cathode (blue plot). Stirring rate: 400 rpm. Electrolysis time: 17 min.

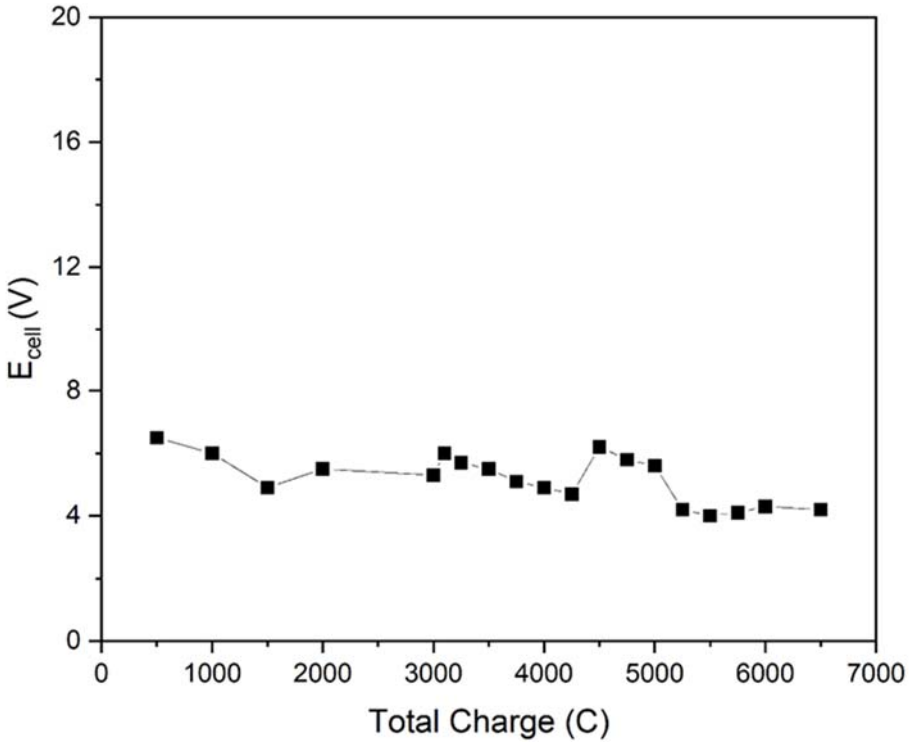

Figure S17. E_{cell} vs total circulated charge corresponding to the first 7 consecutive electrolysis shown in Figure 5a using an IM^{+}_{EE}/GDE cathode at -20 mA/cm^2 in a flow cell type reactor with 1 mM Rh complex in acidic aqueous solution (pH 3.8).

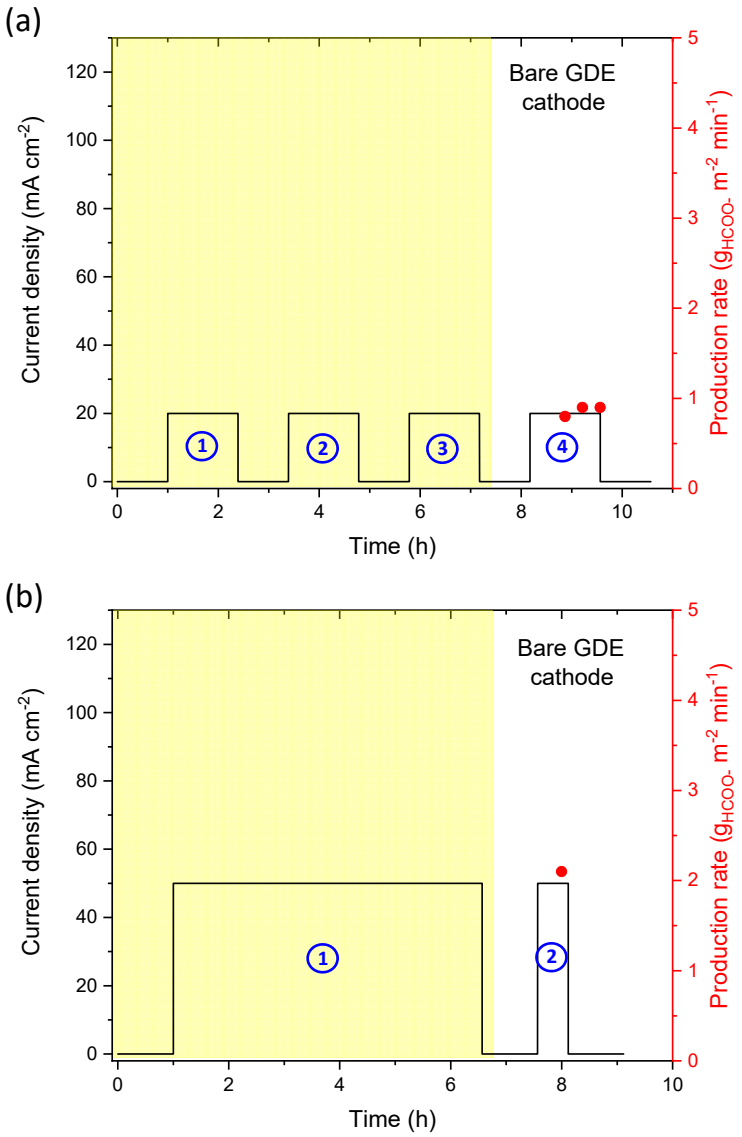

Figure S18. Consecutive CO_2 gas electrolysis performed at different current densities on a bare carbon GDE cathode in acidic aqueous solution (pH 3.8) using 1 mM Rh complex. (a) Four consecutive electrolysis at 20 mA cm^{-2} of 1000 C each and (b) two consecutive electrolysis at 50 mA cm^{-2} of 7000 and 1000 C, respectively. The yellow zone represents the electrochemical cathode activation period.

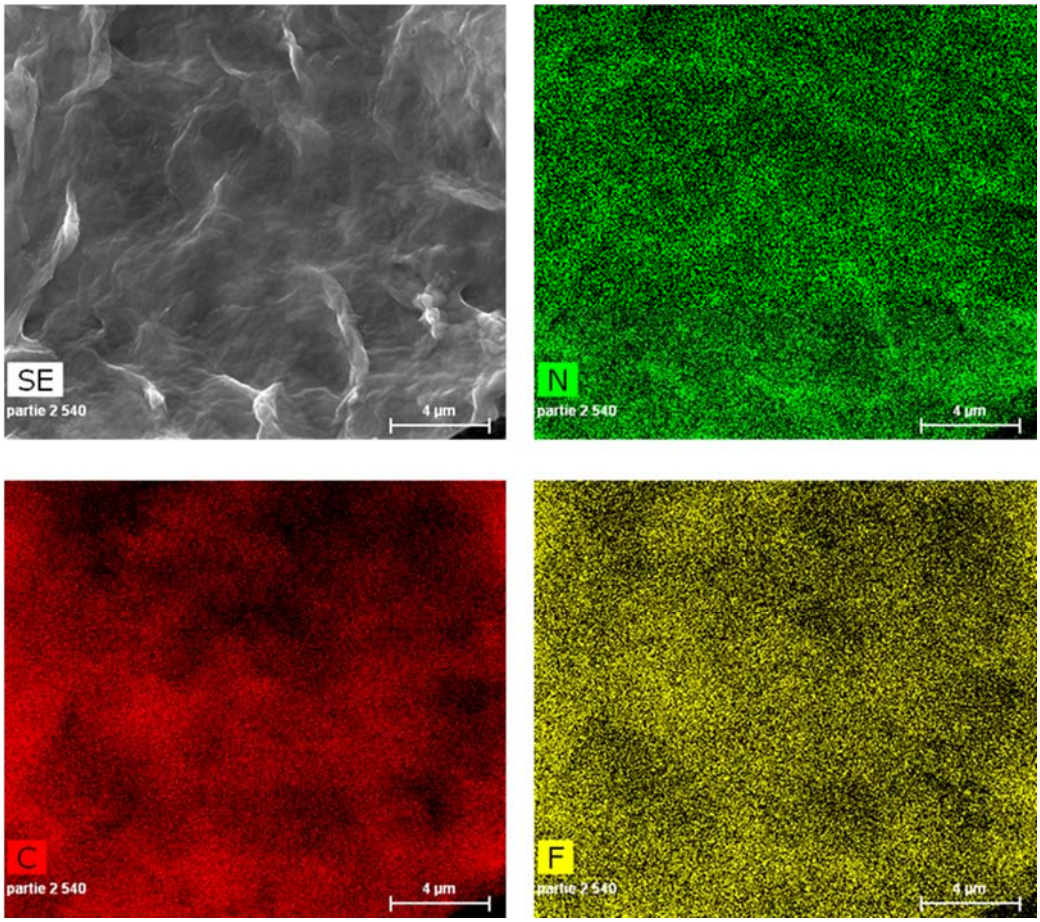

Figure S19. SEM and EDX elemental mapping of IM^{+}_{EE}/GDE cathode N (green), C (red) and F (yellow) after the activation period, which consists of electrolysis in the flow reactor for 3000 C in the acidic catholyte (pH=3.8).

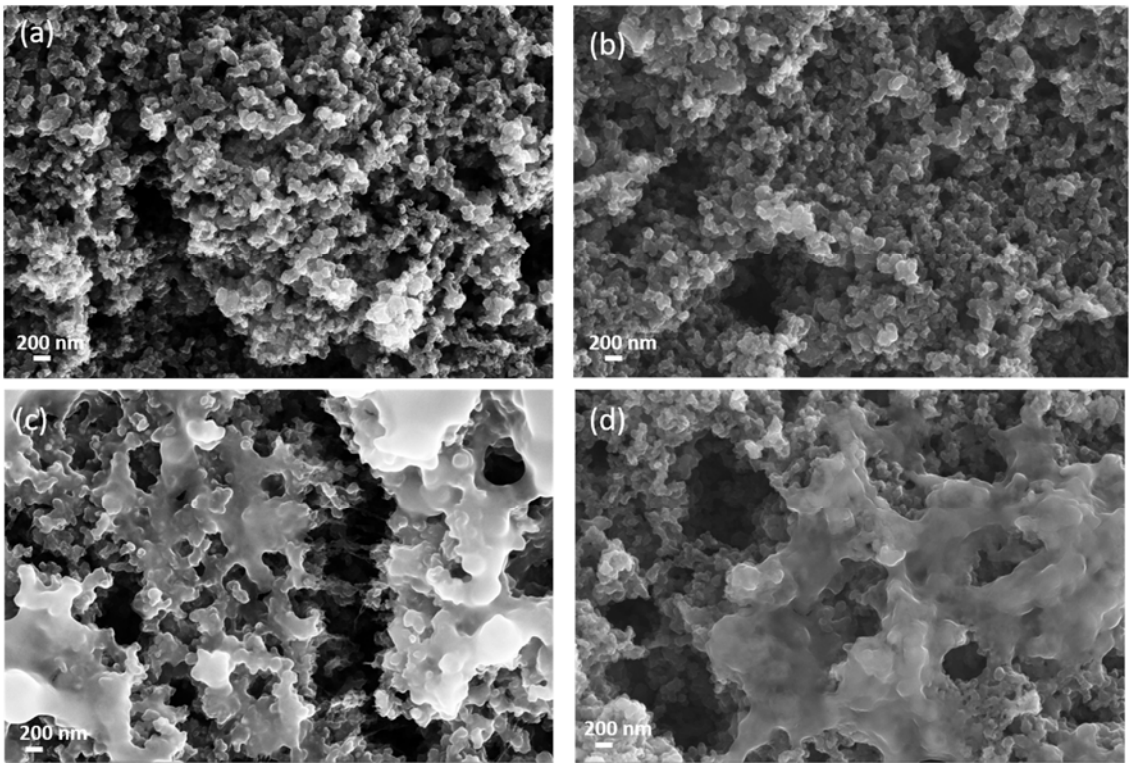

Figure S20. SEM images of (a) GDE cathode, (b) IM^{+}_{EE}/GDE cathode, (c) IM^{+}_{EE}/GDE cathode after activation and (d) IM^{+}_{EE}/GDE cathode after 9 consecutive CO_2RR electrolysis (reported in Figure 5).

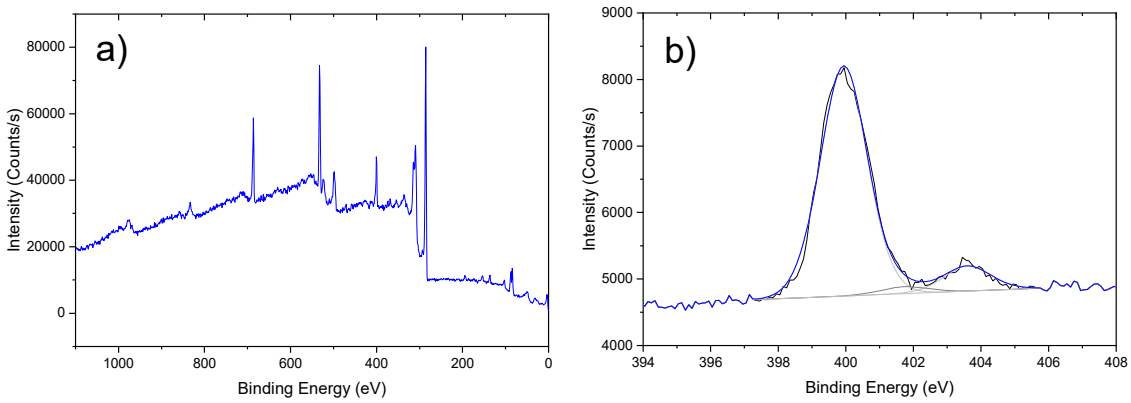

Figure S21. XPS high-resolution spectra survey (a) and N 1s spectra (b) for a modified Au electrode (IM^{+}_{EE}) after CO_2 electrolysis at -3.33 mA/cm^2 (15 C) in CH_3CN/H_2O 95/5 v/v in a H-type cell.

Table S1. Onset and $E_{cat/2}$ potentials from CVs in Figure 4a: 1 mM Rh complex on different cathodes in acetonitrile solution containing 5% v/v H_2O under CO_2.

Cathode	Electrolyte in acetonitrile solution	Onset potential (V) vs Fc^+/Fc	$E_{cat/2}$ (V) vs Fc^+/Fc
Pristine GC	0.5 M [TBA][PF_6]	-1.72	-2.03
Pristine GC	0.5 M [EMIM][PF_6]	-1.64	-1.95
IM^+_{EE} cathode	0.5 M [TBA][PF_6]	-1.62	-1.98
IM^+_{EC} cathode	0.5 M [TBA][PF_6]	-1.66	-2.00

Table S2. Comparison of our electrolysis results for CO_2 conversion to formate in a flow cell type reactor with those on different Sn-based cathodes from the literature under comparable experimental conditions.

Catalyst	Main product	Current density (mA cm^{-2})	Product rate (g m^{-2} min^{-1})	FE_{HCOO^-} (%)	Energy consumption (kWh $kmol^{-1}$)	$EE_{full\ cell}$ (%)	Reference
Sn plate	$HCOO^-$	22	0.83	27	615	9.1	[1]
GDE-100 nm SnO_x NPs*	$HCOO^-$	25	2.4	72	-	-	[2]
GDE-100 nm SnO_x NPs*	$HCOO^-$	50	5.6	79	-	-	[2]
GDE-100 nm SnO_x NPs*	$HCOO^-$	100	10.5	79	-	-	[2]
GDE-15 nm Sn NPs*	$HCOO^-$	90	7.5	60	-	-	[3]
IM^+_{EE}/ GDE Rh complex	$HCOO^-$	20	1.3	46	574	8.0	This work
IM^+_{EE}/ GDE Rh complex	$HCOO^-$	50	3.4	48	818	5.5	This work
IM^+_{EE}/ GDE Rh complex	$HCOO^-$	100	4.6	33	2430	1.9	This work

*NPs stands for nanoparticles.

(-) Not calculated.

Figures of merit:

Onset potential (V), defined for this non-ideal system as the potential at which the current deviates from the non-faradaic regime and increases. It is measured by driving a tangent in the CV.[4]

$E_{cat/2}$ potential (V) corresponds to the half wave catalytic potential from CV.[4]

Faraday efficiency (FE, %) of each reaction product (FE_{HCOO^-} and FE_{H2}) are calculated from the ratio between the charge consumed to form each product and the total circulated charge (equation 1). However, the total circulated charge is corrected to discount the initial three electrons consumed by Rh complex (1 mM in solution), which are necessary to generate its active form. Catalyst activation charge = [number of electrons × Faraday constant × mol of catalyst] = [3 × 96485 × 6.06 × 10^{-6}] =1.82 C.

$$FE\ (\%) = \frac{z\,n\,F}{Q}\ x\ 100 \qquad (1)$$

where *z* represents the number of electrons exchanged to form the desired product (e.g. *z* = 2 for the electroconversion of CO_2 into formate), *n* corresponds to the number of moles produced, F is the Faraday constant (F = 96485 C mol^{-1}) and *Q* represents the total charge (C) circulated through the system, which is obtained by multiplying the current applied in amperes and the electrolysis time in seconds.

The **cathodic half reaction energy efficiency (EE, %)**[5] was calculated for CO_2 conversion to formate reaction according to equation 2:

$$EE_{HCOO^-}\ (\%) = (E^o/E)\ x\ FE_{HCOO^-} \qquad (2)$$

where E^o is the standard thermodynamic potential in volts required for the electrocatalytic reduction of CO_2 to formate, whereas E and FE_{HCOO^-} represent the experimental cathode potential applied in volts and the formate Faradaic Efficiency (%), respectively. $E^o_{CO2/HCOO^-}$ (CH_3CN, H_2O) = -1.32 V *vs.* Fc^+/Fc or $E^o_{CO2/HCOOH}$ (H_2O) = -0.199 V *vs.* RHE in acetonitrile[6] and aqueous solutions[7], respectively. Additionally, $E^o_{CO2/HCOOH}$ in aqueous solution was transferred from RHE to the Ag/AgCl/KCl_{sat} (KCl saturated) reference electrode taking into account the solution pH and using the following equation:

$$E^0_{CO2/HCOOH}(Ag/AgCl) = E^0_{CO2/HCOOH}(RHE) - 0.059\ pH - 0.197$$

Then, $E^o_{CO2/HCOOH}$ *(H_2O)* = -0.62 V *vs.* Ag/AgCl (pH=3.8).

The **full cell energy efficiency ($EE_{full\ cell}$, %)**[8] was calculated on the basis of the cathodic CO_2 to formate reaction at pH of 3.8 (-0.62 V *vs.* Ag/AgCl) coupled with anodic water oxidation reaction ($O_2 + 4H^+ + 4e^- \leftrightarrow 2H_2O$) at pH of 13.7 (0.225 V *vs.* Ag/AgCl).

$$EE_{full\ cell}\ (\%) = (E^o_{full\ cell}/E_{full\ cell})\ x\ FE_{HCOO^-} \qquad (3)$$

where $E^o_{full\ cell}$ is the difference between the standard thermodynamic potentials in volts of the anodic and cathodic reactions considered (0.225 – (-0.62)) = 0.845 V. $E_{full\ cell}$ is the experimental potential difference between cathode and anode in the electrochemical reactor (cell potential in volts).

The **Production Rate (r)**[9] (g m^{-2} min^{-1}) of each reaction product is defined as the productivity (grams) per unit of cathode area (geometric area, m^{-2}) and time (min^{-1}).

$$r_{HCOO^-} = (FE_{HCOO^-}/100) \bullet (j_{total} / z\ F) \bullet 2700 \qquad (4)$$

$$r_{CO} = (FE_{CO}/100) \bullet (j_{total} / z\ F) \bullet 1680 \qquad (5)$$

where *z* represents the number of electrons exchanged to form the desired product (e.g. *z* = 2 for the electroconversion of CO_2 into formate or CO), FE_{HCOO^-} (%), j_{total} (A/m^{-2}), F is the Faraday constant (F = 96485 C mol^{-1}) and the molecular weight of formate is 45 g mol^{-1} and CO is 28 g mol^{-1}.

The **Energy Consumption (EC)**, which represents the required amount of energy used to produce the target product (formate), according to:

$$Energy\ Consumption\ \left(\frac{kWh}{kmol}\right) = \frac{Q \cdot E_{full\ cell}}{n}\ x\ 2.78 \cdot 10^{-4} \qquad (6)$$

References

(1) Alvarez-Guerra, M.; Del Castillo, A.; Irabien, A. Continuous Electrochemical Reduction of Carbon Dioxide into Formate Using a Tin Cathode: Comparison with Lead Cathode. *Chem. Eng. Res. Des.* **2014**, *92* (4), 692–701.

(2) Li, M.; Idros, M. N.; Wu, Y.; Garg, S.; Gao, S.; Lin, R.; Rabiee, H.; Li, Z.; Ge, L.; Rufford, T. E.; Zhu, Z.; Li, L.; Wang, G. Unveiling the Effects of Dimensionality of Tin Oxide-Derived Catalysts on CO $_2$ Reduction by Using Gas-Diffusion Electrodes. *React. Chem. Eng.* **2021**, *6* (2), 345–352.

(3) Del Castillo, A.; Alvarez-Guerra, M.; Solla-Gullón, J.; Sáez, A.; Montiel, V.; Irabien, A. Sn Nanoparticles on Gas Diffusion Electrodes: Synthesis, Characterization and Use for Continuous CO 2 Electroreduction to Formate. *J. CO2 Util.* **2017**, *18*, 222–228.

(4) Appel, A. M.; Helm, M. L. Determining the Overpotential for a Molecular Electrocatalyst. *ACS Catal.* **2014**, *4* (2), 630–633.

(5) Merino-Garcia, I.; Tinat, L.; Albo, J.; Alvarez-Guerra, M.; Irabien, A.; Durupthy, O.; Vivier, V.; Sánchez-Sánchez, C. M. Continuous Electroconversion of CO2 into Formate Using 2 Nm Tin Oxide Nanoparticles. *Appl. Catal. B Environ.* **2021**, *297*, 120447–120458.

(6) Costentin, C.; Drouet, S.; Robert, M.; Savéant, J.-M. A Local Proton Source Enhances CO2 Electroreduction to CO by a Molecular Fe Catalyst. *Science* **2012**, *338* (6103), 90–94.

(7) Bard, A. J.; Parsons, R.; Jordan, J. *Standard Potentials in Aqueous Solution*, 1st ed.; Monographs in electroanalytical chemistry and electrochemistry; M. Dekker: New York, 1985.

(8) Li, F.; Li, Y. C.; Wang, Z.; Li, J.; Nam, D.-H.; Lum, Y.; Luo, M.; Wang, X.; Ozden, A.; Hung, S.-F.; Chen, B.; Wang, Y.; Wicks, J.; Xu, Y.; Li, Y.; Gabardo, C. M.; Dinh, C.-T.; Wang, Y.; Zhuang, T.-T.; Sinton, D.; Sargent, E. H. Cooperative CO2-to-Ethanol Conversion via Enriched Intermediates at Molecule–Metal Catalyst Interfaces. *Nat. Catal.* **2020**, *3* (1), 75–82.

(9) Sen, S.; Brown, S. M.; Leonard, M.; Brushett, F. R. Electroreduction of Carbon Dioxide to Formate at High Current Densities Using Tin and Tin Oxide Gas Diffusion Electrodes. *J. Appl. Electrochem.* **2019**, *49* (9), 917–928.